



PERGAMON

Journal of Quantitative Spectroscopy &
Radiative Transfer 76 (2003) 237–267

Journal of
Quantitative
Spectroscopy &
Radiative
Transfer

www.elsevier.com/locate/jqsrt

The spectrum of acetylene in the 5- μm region from new line-parameter measurements

D. Jacquemart^a, J.-Y. Mandin^a, V. Dana^{a,*}, L. Régalia-Jarlot^b, J.-J. Plateaux^b,
D. Décatoire^b, L.S. Rothman^c

^aLaboratoire de Physique Moléculaire et Applications, Université Pierre-et-Marie-Curie, CNRS, Case courrier 76,
Tour 13, 4, place Jussieu, 75252 Paris Cedex 05, France

^bGroupe de Spectrométrie Moléculaire et Atmosphérique, Université de Reims-Champagne-Ardenne, CNRS,
BP 347, 51062 Reims Cedex, France

^cHarvard-Smithsonian Center for Astrophysics, Atomic and Molecular Physics Division, 60 Garden Street,
02138-1516 Cambridge, MA, USA

Received 23 January 2002; accepted 3 April 2002

Abstract

Using Fourier Transform spectra (unapodized FWHM: 0.002 cm^{-1}) of acetylene $^{12}\text{C}_2\text{H}_2$, absolute line positions have been obtained in the 5- μm region for about 490 lines belonging to 15 hot bands arising from the $v_4 = 1$ or $v_5 = 1$ lower vibrational level, improving the data available in this spectral region. Absolute line intensities have been measured for about 410 lines, from which vibrational transition dipole moments squared could be determined, as well as empirical Herman-Wallis coefficients when it was possible. The self-broadening coefficients of more than 370 lines have been measured at room temperature, showing that no vibrational dependence exists for the bands of acetylene already studied, and allowing a significant determination of their rotational dependence. Furthermore, about 120 measured values of self-shifting coefficients are tentatively proposed. Combining results published for other bands, and using the smoothed line-parameter values obtained in this work, a HITRAN-format line list of the acetylene molecule has been set up in this spectral region.
© 2002 Elsevier Science Ltd. All rights reserved.

Keywords: Acetylene; Infrared; Vibro-rotational transitions; Fourier transform spectroscopy; Transition dipole moment; Line parameters

1. Introduction

The present paper is dedicated to the study of acetylene FT spectra recorded with the Reims interferometer [1,2]. It is the continuation of a previous study [3] in which numerous absolute line

* Corresponding author. Tel.: + 33-1-44-27-44-75; fax: + 33-1-44-27-70-33.

E-mail address: vdana@ccr.jussieu.fr (V. Dana).

parameters, i.e., line positions, self-shifting coefficients, intensities, and self-broadening coefficients, were measured for the cold bands of $^{12}\text{C}_2\text{H}_2$ absorbing in the 5- μm spectral region. This region was first studied by Plíva [4,5]. The set of bands arising in this region are important for theoretical calculations [6,7], since they involve energy levels affected by numerous anharmonic, Coriolis, and ℓ -type resonances. The goal of this effort was to complete the experimental quantitative spectroscopic information in this region, mainly as far as line intensities are concerned. A maximum of line parameters were measured for the 15 remaining hot bands, not studied in Ref. [3]. As a result, 406 intensities were obtained for lines belonging to 9 bands of $^{12}\text{C}_2\text{H}_2$ arising from the $v_4 = 1$ lower vibrational level, and to 6 bands arising from the $v_5=1$ level, allowing the determination of vibrational transition dipole moments squared and band intensities. As no significant vibrational dependence was observed for the self-broadening coefficients, the 371 new values obtained in this work were included in the set of values given in Ref. [3], in order to deduce a polynomial expansion describing the rotational dependence. A synthetic spectrum of the studied bands was generated, combining the line positions calculated by Plíva [4] and those smoothed in this work when it was possible. Line intensities were calculated from our measured values. To make these data more easily usable, we chose to put them in a HITRAN format line list. For that, the best available experimental data were chosen to update the air-broadening and air-shifting coefficients.

2. Experimental procedure and line-parameter measurements

The step-by-step interferometer [1,2] built at GSMA (Reims) was used under the experimental conditions described in Ref. [3]. The characteristics of the 15 recorded spectra can be found in Table 1. A portion of one of the spectra is given in Fig. 1. Let us recall that two filters were used to cover the whole 1800–2260 cm^{-1} spectral region, and that the middle of the region was inaccessible to study, being on the edge of the two filters. A commercial gas sample, furnished by Air Liquide Alphagaz, with a stated purity of 99.55% in natural abundances, was used without further purification. Cross comparisons [3] with line intensities obtained by other authors in a different spectral region led to the conclusion that the amount of $^{12}\text{C}_2\text{H}_2$ in our cell is known with an uncertainty smaller than 2%.

As in Ref. [3], a multispectrum fitting procedure [8] (hereafter denoted as MSF) was used to retrieve line parameters from the spectra. This procedure was found very efficient to complete the previous results [3] when treating weak bands, or lines located in complicated regions of the spectrum. In this work, the MSF method was used in the same conditions as in Ref. [3]. First, the phase error and the effective iris radius needed to calculate an accurate apparatus function were determined for each spectrum. Second, an average self-collisional narrowing coefficient was obtained [3] to calculate an absorption coefficient that takes into account the collisional narrowing, this value being fixed in the final run of the MSF code. An absolute calibration of the wavenumber scales was also performed [3].

3. Results

The results of this work are given in Table 2. The wavenumber calibration allowed the determination of 486 absolute line positions, with a mean accuracy of $\pm 0.0002 \text{ cm}^{-1}$. As in Ref. [3],

Table 1
Experimental conditions and characteristics of the recorded spectra

Commercial sample (Air Liquide Alphagaz)			Region 1	Region 2
Natural C ₂ H ₂ :	97.760% of ¹² C ₂ H ₂			
Stated purity of natural C ₂ H ₂ :	99.55%			
Maximum path difference (cm)		301	261	
Unapodized FWHM resolution limit (10 ⁻³ cm ⁻¹)		1.7	1.9	
Collimator focal length (mm)		1040	1040	
Useful spectral domain (cm ⁻¹)		1800–1950	1940–2260	
Spectrum No. (Region)	Iris radius (mm)	Total pressure ±0.5% (Torr) ^a	Absorbing path (cm)	Temperature ±0.5 K
1 (2) ^b	2.0	20.68	31.19	295.7 ₅
2 (2)	2.05	4.007	816.6	294.4 ₅
3 (1)	2.02	4.004	816.6	294.3 ₅
4 (1)	2.17	4.013	1616.6	294.9 ₅
5 (2) ^c	2.0	4.016	1616.6	294.9 ₅
6 (2)	2.17	10.14	816.6	295.1 ₅
7 (1)	2.16	10.13	816.6	295.0 ₅
8 (1)	2.25	4.043	2416.6	295.6 ₅
9 (2)	2.26	4.043	2416.6	295.6 ₅
10 (2)	2.17	10.20	1616.6	294.9 ₅
11 (1)	2.25	10.20	1616.6	294.9 ₅
12 (1)	2.2 ^d	49.9	416.6	295.4 ₅
13 (2)	2.2 ^d	49.9	416.6	292.2 ₅
14 (2)	2.29	10.12	2416.6	294.9 ₅
15 (1)	2.30	10.11	2416.6	294.8 ₅

^a1 Torr = 1.333 hPa.

^bThis preliminary spectrum, recorded with a weak optical depth, was not used in the final treatment.

^cThis spectrum could not be used in the final treatment, because of a small experimental defect.

^dAverage effective iris radius.

the line positions of each sub-band were adjusted, each time that it was possible, by polynomial expansions in order to check the assignments. For that, the *P* and *R* branches of each sub-band were fitted simultaneously, and the *Q* branch separately. (As they are effective, the coefficients obtained for these polynomial expansions are not given here.) Note that the line positions of the *Pee* and *Ree* sub-branches of the (3v₄ + v₅)²II – v₄¹ band cannot be adjusted simultaneously, because of strong interactions already pointed out by Plíva [4]. On the whole, the comparison with Plíva's experimental line positions [4] is quite good, and his extrapolations allowed the assignment of new lines for some of the bands.

Absolute line intensities were measured for 406 lines (see Table 2). The precision is between about ±3 to ±5%, and the accuracy in absolute values is on the average ±5% [3]. The formalism and the relation used to calculate the transition dipole moment squared from the line intensity are the same as those used in previous works (see Eqs. (1)–(6) of Ref. [9]), and the partition function was calculated using the polynomial expansion given by Gamache et al. [10]. The transition dipole

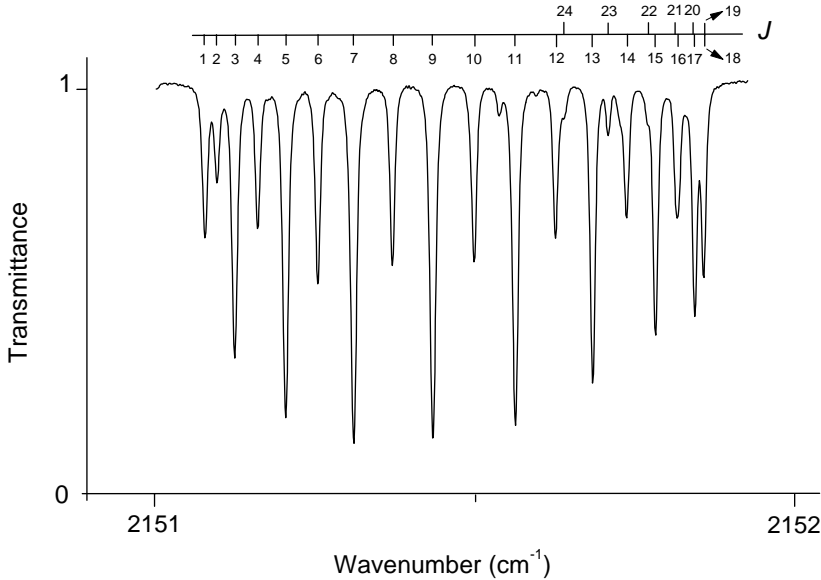


Fig. 1. Portion of spectrum 14 of Table 1, showing the Q branch of the $4v_5^0 - v_5^1$ band, exhibiting a branch head at $J = 19$, around 2151.9 cm^{-1} . Note the intensity alternation of the $^{12}\text{C}_2\text{H}_2$ lines, and the presence of a few $^{12}\text{C}^{13}\text{CH}_2$ lines.

moments squared have been plotted in Figs. 2–11 for some bands. When it was possible, significant empirical Herman-Wallis coefficients were deduced, without taking into account the resonances. The Herman-Wallis factors were expanded as

$$F^{RP}(m) = [1 + A_1^{RP}m + A_2^{RP}m^2] \quad (1)$$

for P and R branches, m being equal to $J + 1$ in the R branch, and $-J$ in the P branch; and for a Q branch, with m equal to J

$$F^Q(m) = [1 + A_2^Q m(m + 1)]. \quad (2)$$

Note that the terms between brackets are not squared. The band centers and Herman-Wallis coefficients are given in Table 3, together with the vibrational dipole moments squared, and band intensities calculated using Eq. (10) of Ref. [9]. In Table 3, the results obtained in Ref. [3] for the 3 cold bands have also been recalled. Note that for one band with ℓ -type doubling, the two sub-bands could be treated separately. For a few bands, the number of measured line intensities was too weak to allow the determination of Herman-Wallis coefficients, but we thought it useful to deduce, tentatively, values of vibrational transition dipole moments in order to perform predictive calculations of transition dipole moment squared values.

As can be seen in Fig. 10, the simultaneous adjustment of the Pee , Ree , and Qef branches of the $4v_5^0 - v_5^1$ band (see Fig. 1) is difficult, the Qef low- J lines leading to a vibrational transition dipole moment squared noticeably smaller than for Pee and Ree branches. We checked carefully that for

Table 2

Line parameters obtained for 15 hot bands of $^{12}\text{C}_2\text{H}_2$ in the 5- μm spectral region^a

Line	σ_{obs}	$k_{\sigma}^N_{\text{obs}}$	$k_{\sigma}^N_{\text{calc}}$	o–c%	$ R _{\text{obs}}^2$	$\gamma_{\text{self obs}}^0$
$(3v_4 + v_5)_+^0 - v_4^1$						
$Qff20$	1951.49101	1.03D–23	1.02D–23	0.97	1.85D–05	0.1340
$(3v_4 + v_5)_-^0 - v_4^1$						
$Qfe\ 4$	1972.30691	1.74D–24	1.67D–24	4.02	4.26D–06	—
$Qfe\ 5$	1972.37238	5.69D–24	5.87D–24	−3.16	4.02D–06	0.1611
$Qfe\ 6$	1972.44668	2.28D–24	2.19D–24	3.95	4.38D–06	0.1605
$Qfe\ 7$	1972.52825	6.65D–24	7.13D–24	−7.22	4.00D–06	0.1471
$Qfe\ 9$	1972.70409	8.08D–24	7.74D–24	4.21	4.66D–06	0.1537
$Qfe10$	1972.79556	2.79D–24	2.60D–24	6.81	4.90D–06	0.1411
$Qfe11$	1972.88785	8.31D–24	7.73D–24	6.98	5.03D–06	0.155
$Qfe12$	1972.97936	2.24D–24	2.51D–24	−12.05	4.29D–06	—
$Qfe13$	1973.07157	6.97D–24	7.20D–24	−3.30	4.78D–06	0.1391
$Rff\ 6$	1988.76038	1.77D–24	2.09D–24	−18.08	2.44D–06	0.1547
$Rff10$	1998.16100	1.17D–24	1.02D–24	12.82	1.42D–06	0.1450
$(3v_4 + v_5)^2\text{II} - v_4^1$						
$Pee\ 9$	1924.43559	1.01D–23	1.13D–23	−11.88	3.65D–05	0.1438
$Pee11$	1919.93952	1.15D–23	1.21D–23	−5.22	4.04D–05	0.1538
$Pee13$	1915.44460	1.17D–23	1.18D–23	−0.85	4.41D–05	0.1505
$Pee15$	1910.93702	1.08D–23	1.06D–23	1.85	4.74D–05	0.1441
$Pee17$	1906.40816	9.19D–24	8.78D–24	4.46	5.06D–05	0.1390
$Pee19$	1901.85420	7.14D–24	6.85D–24	4.06	5.27D–05	0.1283
$Pee21$	1897.27439	5.17D–24	5.03D–24	2.71	5.44D–05	0.1196
$Pee23$	1892.66951	3.55D–24	3.49D–24	1.69	5.63D–05	0.1143
$Pee27$	1883.38747	1.37D–24	1.42D–24	−3.65	5.83D–05	0.1021
$Ree\ 3$	1954.65251	1.45D–23	1.69D–23	−16.55	2.74D–05	0.1888
$Ree\ 5$	1959.50405	1.62D–23	1.84D–23	−13.58	2.72D–05	0.1740
$Ree\ 9$	1969.28797	1.82D–23	1.76D–23	3.30	3.02D–05	0.1758
$Ree13$	1979.06574	1.33D–23	1.31D–23	1.50	2.87D–05	0.1457
$Ree17$	1988.74504	7.83D–24	7.76D–24	0.89	2.77D–05	0.1305
$Ree19$	1993.53792	5.57D–24	5.54D–24	0.54	2.74D–05	0.1288
$Ree21$	1998.29918	3.60D–24	3.77D–24	−4.72	2.59D–05	0.1185
$Ree22$	2000.66805	9.80D–25	1.02D–24	−4.08	2.62D–05	0.1213
$Ree23$	2003.02909	2.34D–24	2.44D–24	−4.27	2.61D–05	0.1133
$Ree24$	2005.38241	5.71D–25	6.44D–25	−12.78	2.41D–05	0.1023
$Pff\ 8$	1926.35236	7.54D–24	7.72D–24	−2.39	2.91D–05	0.1647
$Pff12$	1917.09168	8.67D–24	8.59D–24	0.92	3.12D–05	0.1547
$Pff14$	1912.48543	7.83D–24	7.78D–24	0.64	3.17D–05	0.1492
$Pff18$	1903.31092	5.26D–24	5.08D–24	3.42	3.36D–05	0.1355
$Pff20$	1898.73723	3.72D–24	3.72D–24	0.00	3.29D–05	0.1194
$Pff26$	1885.03289	1.01D–24	1.03D–24	−1.98	3.35D–05	0.1043
$Rff\ 4$	1956.97997	1.43D–23	1.46D–23	−2.10	2.52D–05	0.1730
$Rff\ 9$	1968.96809	4.77D–24	4.77D–24	0.00	2.39D–05	0.1587

(continued on next page)

Table 2 (continued)

Line	σ_{obs}	$k_{\sigma}^N_{\text{obs}}$	$k_{\sigma}^N_{\text{calc}}$	o–c%	$ R _{\text{obs}}^2$	$\gamma_{\text{self obs}}^0$
Rff10	1971.37664	1.35D–23	1.35D–23	0.00	2.35D–05	0.1500
Rff12	1976.20223	1.15D–23	1.15D–23	0.00	2.29D–05	0.1433
Rff14	1981.03696	8.96D–24	9.12D–24	−1.79	2.15D–05	0.1397
Rff16	1985.87757	7.05D–24	6.85D–24	2.84	2.17D–05	0.1332
Rff18	1990.72098	4.85D–24	4.85D–24	0.00	2.02D–05	0.1267
Rff20	1995.56303	3.21D–24	3.24D–24	−0.93	1.92D–05	0.1224
Rff21	1997.98229	8.66D–25	8.67D–25	−0.12	1.89D–05	0.1218
Rff22	2000.39978	2.01D–24	2.05D–24	−1.99	1.81D–05	0.1095
Rff24	2005.22692	1.26D–24	1.23D–24	2.38	1.81D–05	0.1173
$(3v_4 + v_5)^2I - v_4^1$						
Ree 9	1997.49134	1.76D–24	1.66D–24	5.68	2.88D–06	0.1547
Ree10	1999.97071	4.19D–25	4.47D–25	−6.68	2.15D–06	—
Rff 9	1997.18193	1.10D–24	1.13D–24	−2.73	5.43D–06	0.1623
Rff10	1999.61650	3.34D–24	3.36D–24	−0.60	5.73D–06	0.1511
Rff11	2002.05801	1.09D–24	1.09D–24	0.00	5.95D–06	0.1470
$v_2 + v_5^1 - v_4^1$						
Pee 2	2085.50461	5.93D–25	5.60D–25	5.56	7.61D–06	0.2030
Pee 3	2083.13324	2.90D–24	2.89D–24	0.34	7.22D–06	0.1896
Pee 4	2080.75264	1.30D–24	1.30D–24	0.00	7.25D–06	0.1838
Pee 5	2078.36110	4.89D–24	4.70D–24	3.89	7.51D–06	0.1866
Pee 6	2075.95998	1.75D–24	1.78D–24	−1.71	7.11D–06	0.1553
Pee 8	2071.12740	2.05D–24	2.03D–24	0.98	7.37D–06	0.1546
Pee 9	2068.69628	6.21D–24	6.20D–24	0.16	7.30D–06	0.1563
Pee10	2066.25520	2.04D–24	2.05D–24	−0.49	7.26D–06	0.1509
Pee11	2063.80453	6.01D–24	5.99D–24	0.33	7.33D–06	0.1463
Pee12	2061.34402	1.93D–24	1.90D–24	1.55	7.44D–06	0.1481
Pee13	2058.87347	5.36D–24	5.34D–24	0.37	7.36D–06	0.1452
Pee14	2056.39336	1.70D–24	1.64D–24	3.53	7.64D–06	0.1422
Pee15	2053.90375	4.41D–24	4.44D–24	−0.68	7.31D–06	0.1375
Pee16	2051.40431	1.28D–24	1.32D–24	−3.13	7.17D–06	0.1314
Pee17	2048.89545	3.36D–24	3.46D–24	−2.98	7.19D–06	0.1287
Pee18	2046.37692	9.92D–25	9.95D–25	−0.30	7.39D–06	0.1346
Pee19	2043.84896	2.53D–24	2.54D–24	−0.40	7.38D–06	0.1245
Pee21	2038.76448	1.71D–24	1.76D–24	−2.92	7.23D–06	0.1133
Ree 2	2097.20612	—	9.92D–25	—	—	—
Ree13	2122.03232	5.68D–24	5.63D–24	0.88	7.02D–06	0.1407
Ree14	2124.22547	—	1.71D–24	—	—	—
Ree15	2126.40764	4.67D–24	4.62D–24	1.07	7.01D–06	0.1335
Ree16	2128.57914	1.35D–24	1.36D–24	−0.74	6.87D–06	0.1330
Ree18	2132.88897	1.05D–24	1.02D–24	2.86	7.08D–06	—
Pff 2	2085.48245	1.69D–24	1.68D–24	0.59	7.21D–06	0.1987
Pff 3	2083.09866	9.37D–25	9.64D–25	−2.88	7.01D–06	0.1851
Pff 4	2080.70395	3.88D–24	3.89D–24	−0.26	7.20D–06	0.1786

Table 2 (continued)

Line	σ_{obs}	$k_{\sigma \text{ obs}}^N$	$k_{\sigma \text{ calc}}^N$	o–c%	$ R _{\text{obs}}^2$	$\gamma_{\text{self obs}}^0$
Pff 6	2075.88097	5.29D–24	5.35D–24	–1.13	7.19D–06	0.1623
Pff 7	2073.45290	1.93D–24	1.94D–24	–0.52	7.26D–06	0.1595
Pff 8	2071.01380	6.12D–24	6.09D–24	0.49	7.33D–06	0.1580
Pff 9	2068.56370	2.09D–24	2.07D–24	0.96	7.40D–06	0.1560
Pff 10	2066.10263	6.27D–24	6.17D–24	1.59	7.45D–06	0.1561
Pff 11	2063.63080	1.97D–24	2.00D–24	–1.52	7.25D–06	0.1455
Pff 12	2061.14798	5.74D–24	5.72D–24	0.35	7.39D–06	0.1476
Pff 14	2056.15000	4.92D–24	4.92D–24	0.00	7.40D–06	0.1414
Pff 15	2053.63583	—	1.48D–24	—	—	—
Pff 16	2051.10914	3.93D–24	3.95D–24	–0.51	7.40D–06	0.1355
Pff 17	2048.57299	—	1.15D–24	—	—	—
Pff 18	2046.02567	2.96D–24	2.98D–24	–0.68	7.41D–06	0.1296
Pff 19	2043.46785	8.54D–25	8.46D–25	0.94	7.56D–06	0.1248
Pff 20	2040.90001	2.11D–24	2.13D–24	–0.95	7.44D–06	0.1221
Pff 21	2038.32139	—	5.86D–25	—	—	—
Rff 2	2097.23112	3.04D–24	2.97D–24	2.30	7.28D–06	0.1940
Rff 4	2101.85096	4.90D–24	4.92D–24	–0.41	7.04D–06	0.1700
Rff 7	2108.69426	2.21D–24	2.18D–24	1.36	7.11D–06	0.1554
Rff 13	2122.06591	1.83D–24	1.86D–24	–1.64	6.83D–06	0.1379
Rff 14	2124.25333	5.09D–24	5.08D–24	0.20	6.91D–06	0.1408
Rff 15	2126.42868	1.52D–24	1.52D–24	0.00	6.89D–06	0.1301
Rff 16	2128.59227	3.98D–24	4.02D–24	–1.01	6.78D–06	0.1320
Rff 18	2132.88475	—	3.00D–24	—	—	—
$(v_4 + 3v_5)_+^0 - v_4^1$						
Pee 1	2143.75278	—	1.35D–24	—	—	—
Pee 11	2121.26792	4.34D–24	4.43D–24	–2.07	4.68D–06	0.1427
Pee 12	2119.10248	—	1.43D–24	—	—	—
Pee 13	2116.94732	3.98D–24	4.08D–24	–2.51	4.91D–06	0.1402
Pee 14	2114.80007	—	1.27D–24	—	—	—
Pee 15	2112.65948	3.52D–24	3.53D–24	–0.28	5.30D–06	0.1373
Pee 16	2110.52345	1.07D–24	1.07D–24	0.00	5.45D–06	0.1336
Pee 17	2108.39073	2.89D–24	2.89D–24	0.00	5.65D–06	0.1338
$Qef 1$						
Qef 2	2146.11288	—	6.74D–25	—	—	—
Qef 3	2146.13234	3.20D–24	3.28D–24	–2.50	3.99D–06	0.1898
Qef 4	2146.15979	1.46D–24	1.46D–24	0.00	4.02D–06	0.1793
Qef 5	2146.19594	5.24D–24	5.34D–24	–1.91	3.93D–06	0.1678
Qef 6	2146.24009	—	2.02D–24	—	—	—
Qef 7	2146.29050	6.51D–24	6.59D–24	–1.23	3.83D–06	0.1584
Qef 8	2146.40888	6.93D–24	6.94D–24	–0.14	3.71D–06	0.1520
Qef 9	2146.47400	2.37D–24	2.27D–24	4.22	3.77D–06	0.1652
Qef 10	2146.54134	6.56D–24	6.50D–24	0.91	3.53D–06	0.1521
Qef 11	2146.60920	1.99D–24	2.02D–24	–1.51	3.33D–06	0.1462
Qef 12	2146.67628	5.34D–24	5.50D–24	–3.00	3.14D–06	0.1383
Qef 13	2146.74032	—	1.63D–24	—	—	—
Qef 15	2146.85428	—	1.20D–24	—	—	—

(continued on next page)

Table 2 (continued)

Line	σ_{obs}	$k_{\sigma}^N_{\text{obs}}$	$k_{\sigma}^N_{\text{calc}}$	O–C%	$ R _{\text{obs}}^2$	$\gamma_{\text{self obs}}^0$
$Q_{\text{ef}16}$	2146.89942	3.04D–24	2.99D–24	1.64	2.64D–06	0.1510
$Q_{\text{ef}17}$	2146.93422	—	8.05D–25	—	—	—
$Q_{\text{ef}18}$	2146.96058	—	1.90D–24	—	—	—
$Ree\ 3$	2155.70253	—	1.95D–24	—	—	—
$Ree\ 4$	2158.14893	—	8.36D–25	—	—	—
$Ree\ 7$	2165.58698	3.84D–24	3.73D–24	2.86	4.51D–06	0.1573
$Ree\ 8$	2168.09412	—	1.32D–24	—	—	—
$Ree10$	2173.14717	—	1.39D–24	—	—	—
$Ree13$	2180.78805	3.87D–24	3.87D–24	0.00	4.98D–06	0.1319
$Ree15$	2185.90288	3.52D–24	3.39D–24	3.69	5.47D–06	0.1371
$Ree17$	2191.01849	2.68D–24	2.81D–24	−4.85	5.33D–06	0.1113
$Ree18$	2193.57284	8.46D–25	8.32D–25	1.65	5.85D–06	0.1246
$Ree19$	2196.12315	2.30D–24	2.19D–24	4.78	6.23D–06	0.1080
$Ree20$	2198.66847	6.04D–25	6.33D–25	−4.80	5.86D–06	0.1186
$(v_4 + 3v_5)^0 - v_4^1$						
$P_{\text{ff}\ 7}$	2155.58657	2.15D–24	2.27D–24	−5.58	6.66D–06	—
$P_{\text{ff}\ 9}$	2150.97231	2.39D–24	2.40D–24	−0.42	7.21D–06	0.1476
$P_{\text{ff}14}$	2139.52538	6.54D–24	5.86D–24	10.40	8.78D–06	0.1524
$P_{\text{ff}18}$	2130.41564	3.79D–24	3.77D–24	0.53	8.61D–06	0.1265
$P_{\text{ff}19}$	2128.13883	1.10D–24	1.09D–24	0.91	8.83D–06	0.1260
$P_{\text{ff}20}$	2125.86112	2.79D–24	2.78D–24	0.36	8.98D–06	0.1379
$P_{\text{ff}21}$	2123.58147	7.62D–25	7.82D–25	−2.62	8.94D–06	0.1140
$P_{\text{ff}22}$	2121.29928	1.96D–24	1.95D–24	0.51	9.44D–06	0.1007
$P_{\text{ff}24}$	2116.72697	1.27D–24	1.30D–24	−2.36	9.69D–06	0.1074
$P_{\text{ff}26}$	2112.14035	8.15D–25	8.21D–25	−0.74	1.03D–05	0.1114
$Q_{\text{fe}\ 4}$	2172.13684	3.25D–24	2.96D–24	8.92	7.23D–06	—
$Q_{\text{fe}\ 6}$	2172.33160	3.63D–24	3.68D–24	−1.38	6.33D–06	0.1606
$Q_{\text{fe}\ 7}$	2172.45459	1.14D–23	1.16D–23	−1.75	6.24D–06	0.1547
$Q_{\text{fe}\ 9}$	2172.74866	1.19D–23	1.17D–23	1.68	6.20D–06	0.1708
$Q_{\text{fe}10}$	2172.91866	3.99D–24	3.74D–24	6.27	6.36D–06	0.1694
$Q_{\text{fe}11}$	2173.10322	1.01D–23	1.06D–23	−4.95	5.55D–06	0.1410
$Q_{\text{fe}14}$	2173.73697	—	2.59D–24	—	—	—
$Q_{\text{fe}15}$	2173.97157	6.37D–24	6.73D–24	−5.65	4.81D–06	0.1230
$Q_{\text{fe}18}$	2174.73790	1.25D–24	1.29D–24	−3.20	4.24D–06	0.1166
$Q_{\text{fe}19}$	2175.01153	3.20D–24	3.10D–24	3.13	4.26D–06	0.1332
$Q_{\text{fe}20}$	2175.29265	7.31D–25	8.08D–25	−10.53	3.49D–06	0.0974
$Q_{\text{fe}21}$	2175.58083	—	2.00D–24	—	—	—
$Q_{\text{fe}22}$	2175.87561	5.27D–25	5.43D–25	−3.04	3.75D–06	0.1225
$R_{\text{ff}\ 3}$	2181.47562	9.94D–25	1.06D–24	−6.64	6.31D–06	0.1646
$R_{\text{ff}\ 4}$	2183.87312	3.99D–24	4.07D–24	−2.01	6.63D–06	0.1731
$R_{\text{ff}\ 5}$	2186.27704	1.58D–24	1.61D–24	−1.90	6.67D–06	0.1594
$R_{\text{ff}\ 6}$	2188.68727	5.33D–24	5.47D–24	−2.63	6.68D–06	0.1510
$R_{\text{ff}\ 8}$	2193.52333	6.46D–24	6.27D–24	2.94	7.18D–06	0.1609
$R_{\text{ff}\ 9}$	2195.94818	2.27D–24	2.15D–24	5.29	7.47D–06	0.1620

Table 2 (continued)

Line	σ_{obs}	$k_{\sigma}^N_{\text{obs}}$	$k_{\sigma}^N_{\text{calc}}$	O–C%	$ R _{\text{obs}}^2$	$\gamma_{\text{self obs}}^0$
Rff10	2198.37662	6.54D–24	6.47D–24	1.07	7.23D–06	0.1549
Rff12	2203.24185	6.25D–24	6.15D–24	1.60	7.47D–06	0.1437
Rff13	2205.67688	1.94D–24	1.95D–24	−0.52	7.43D–06	0.1351
Rff14	2208.11250	5.63D–24	5.45D–24	3.20	7.85D–06	0.1388
Rff15	2210.54797	1.68D–24	1.67D–24	0.60	7.77D–06	0.1386
Rff17	2215.41442	1.37D–24	1.35D–24	1.46	8.18D–06	0.1296
Rff19	2220.27109	1.02D–24	1.03D–24	−0.98	8.29D–06	0.1178
Rff20	2222.69356	2.65D–24	2.65D–24	0.00	8.55D–06	0.1179
Rff21	2225.11162	7.21D–25	7.48D–25	−3.74	8.47D–06	0.1082
Rff22	2227.52454	1.81D–24	1.87D–24	−3.31	8.69D–06	0.1108
Rff23	2229.93214	5.34D–25	5.14D–25	3.75	9.56D–06	0.1139
Rff24	2232.33222	—	1.25D–24	—	—	—
$(v_4 + 3v_5)^2 \text{II} - v_4^1$						
Pee 5	2145.19522	8.47D–25	9.30D–25	−9.80	5.05D–06	0.1719
Pee 7	2140.71162	1.42D–24	1.36D–24	4.23	5.50D–06	—
Pee 9	2136.31818	1.58D–24	1.52D–24	3.80	5.12D–06	—
Pee15	2123.75708	7.88D–25	8.56D–25	−8.63	3.11D–06	0.1427
Qfe 3	2156.86984	2.60D–24	2.64D–24	−1.54	5.72D–06	0.1985
Qfe 5	2157.03975	4.08D–24	4.20D–24	−2.94	5.66D–06	0.1781
Qfe 6	2157.15237	—	1.58D–24	—	—	—
Qfe 9	2157.60177	5.29D–24	5.39D–24	−1.89	5.70D–06	0.1618
Qfe10	2157.78734	1.85D–24	1.78D–24	3.78	6.06D–06	0.1508
Qfe11	2157.99124	4.92D–24	5.17D–24	−5.08	5.53D–06	0.1430
Qfe12	2158.21234	1.55D–24	1.64D–24	−5.81	5.52D–06	0.1336
Qfe13	2158.45079	4.87D–24	4.59D–24	5.75	6.18D–06	0.1354
Qfe14	2158.70606	—	1.40D–24	—	—	—
Qfe15	2158.97866	3.70D–24	3.79D–24	−2.43	5.68D–06	0.1325
Qfe16	2159.26748	—	1.12D–24	—	—	—
Qfe20	2160.57872	6.68D–25	6.01D–25	10.03	6.46D–06	0.1420
Qfe21	2160.94237	—	1.49D–24	—	—	—
Ree 9	2181.36715	3.02D–24	3.15D–24	−4.30	4.53D–06	0.1561
Ree10	2183.95424	9.65D–25	9.60D–25	0.52	4.53D–06	0.1694
Ree11	2186.56900	2.35D–24	2.57D–24	−9.36	3.89D–06	0.1475
Ree13	2191.88594	1.86D–24	1.90D–24	−2.15	3.62D–06	0.1516
Ree14	2194.59014	—	5.23D–25	—	—	—
Ree15	2197.32838	1.23D–24	1.26D–24	−2.44	2.97D–06	0.1449
Ree16	2200.10029	3.30D–25	3.25D–25	1.52	2.73D–06	0.1285
Ree17	2202.90701	8.67D–25	7.24D–25	16.49	2.76D–06	0.1486
Ree18	2205.74827	—	1.70D–25	—	—	—
Ree21	2214.49958	—	8.92D–26	—	—	—
Pff 8	2138.10390	—	1.60D–24	—	—	—
Pff10	2133.52691	1.89D–24	1.72D–24	8.99	5.96D–06	0.1704
Pff12	2128.98000	1.62D–24	1.63D–24	−0.62	5.24D–06	0.1386
Pff14	2124.46331	1.45D–24	1.40D–24	3.45	5.27D–06	0.1404

(continued on next page)

Table 2 (continued)

Line	σ_{obs}	k_{σ}^N obs	k_{σ}^N calc	o–c%	$ R _{\text{obs}}^2$	$\gamma_{\text{self obs}}^0$
Pff20	2111.07756	—	5.49D–25	—	—	—
Qef 2	2156.78218	1.58D–24	1.58D–24	0.00	5.88D–06	0.1956
Qef 4	2156.84337	3.47D–24	3.61D–24	−4.03	5.75D–06	0.1840
Qef 5	2156.88868	1.50D–24	1.46D–24	2.67	6.24D–06	0.1899
Qef 8	2157.09123	5.74D–24	5.89D–24	−2.61	6.29D–06	0.1559
Qef 9	2157.18433	—	2.04D–24	—	—	—
Qef10	2157.29236	6.04D–24	6.23D–24	−3.15	6.60D–06	0.1376
Qef12	2157.55739	6.00D–24	6.07D–24	−1.17	7.13D–06	0.1451
Qef13	2157.71763	—	1.95D–24	—	—	—
Qef15	2158.10016	1.65D–24	1.72D–24	−4.24	7.66D–06	0.1278
Qef16	2158.32514	4.79D–24	4.74D–24	1.04	8.33D–06	0.1380
Qef17	2158.57523	—	1.43D–24	—	—	—
Qef18	2158.84953	3.65D–24	3.84D–24	−5.21	8.43D–06	0.1253
Qef19	2159.15019	1.15D–24	1.13D–24	1.74	9.38D–06	0.1296
Rff 3	2166.28463	—	1.13D–24	—	—	—
Rff 7	2175.94330	1.38D–24	1.28D–24	7.25	6.04D–06	0.1850
Rff 8	2178.37623	3.47D–24	3.76D–24	−8.36	5.08D–06	0.1579
Rff 9	2180.81719	1.14D–24	1.21D–24	−6.14	5.16D–06	0.1540
Rff13	2190.64703	8.06D–25	8.71D–25	−8.06	4.73D–06	0.1419
Rff14	2193.11961	2.31D–24	2.31D–24	0.00	5.01D–06	0.1445
Rff15	2195.59698	—	6.69D–25	—	—	—
Rff16	2198.08092	1.75D–24	1.72D–24	1.71	4.87D–06	0.1447
Rff17	2200.56769	4.88D–25	4.81D–25	1.43	4.71D–06	—
Rff19	2205.55717	3.20D–25	3.25D–25	−1.56	4.30D–06	—
Rff21	2210.56865	—	2.06D–25	—	—	—
$(v_4 + 3v_5)^2I - v_4^1$						
Pee 7	2162.98253	1.51D–24	1.52D–24	−0.66	5.81D–06	0.1795
Pee 9	2158.54474	—	1.79D–24	—	—	—
Pee11	2154.17754	—	1.82D–24	—	—	—
Pee13	2149.88209	1.67D–24	1.66D–24	0.60	5.58D–06	0.1433
Pee15	2145.65806	1.50D–24	1.39D–24	7.33	5.86D–06	—
Qfe 2	2179.12336	—	5.42D–25	—	—	—
Qfe 4	2179.24463	—	1.24D–24	—	—	—
Qfe 5	2179.33262	4.47D–24	4.54D–24	−1.57	6.12D–06	0.1714
Qfe 6	2179.43912	1.84D–24	1.74D–24	5.43	6.72D–06	—
Qfe 7	2179.56449	5.61D–24	5.73D–24	−2.14	6.33D–06	0.1590
Qfe 8	2179.70894	2.00D–24	2.04D–24	−2.00	6.48D–06	0.1510
Qfe 9	2179.87306	6.25D–24	6.37D–24	−1.92	6.67D–06	0.1515
Qfe13	2180.73866	—	6.12D–24	—	—	—
Qfe15	2181.30591	5.52D–24	5.43D–24	1.63	8.37D–06	0.1446
Qfe16	2181.62628	1.68D–24	1.67D–24	0.60	8.60D–06	0.1341
Qfe17	2181.97148	4.78D–24	4.54D–24	5.02	9.35D–06	0.1418
Qfe18	2182.34272	—	1.35D–24	—	—	—

Table 2 (continued)

Line	σ_{obs}	$k_{\sigma}^N \text{ obs}$	$k_{\sigma}^N \text{ calc}$	o–c%	$ R _{\text{obs}}^2$	$\gamma_{\text{self obs}}^0$
<i>Qfe19</i>	2182.74079	3.67D–24	3.59D–24	2.18	9.80D–06	0.1292
<i>Qfe20</i>	2183.16673	—	1.04D–24	—	—	—
<i>Qfe21</i>	2183.61912	2.73D–24	2.68D–24	1.83	1.05D–05	0.1261
<i>Qfe22</i>	2184.10089	—	7.59D–25	—	—	—
<i>Qfe23</i>	2184.61067	1.86D–24	1.90D–24	−2.15	1.10D–05	0.1185
<i>Qfe24</i>	2185.14992	5.10D–25	5.24D–25	−2.75	1.14D–05	0.1182
<i>Ree 4</i>	2191.08281	—	1.24D–24	—	—	—
<i>Ree 5</i>	2193.53756	—	3.91D–24	—	—	—
<i>Ree 6</i>	2196.00879	—	1.33D–24	—	—	—
<i>Ree 7</i>	2198.49740	3.86D–24	4.02D–24	−4.15	5.55D–06	0.1620
<i>Ree 8</i>	2201.00310	1.26D–24	1.32D–24	−4.76	5.49D–06	0.1582
<i>Ree 9</i>	2203.52593	3.71D–24	3.84D–24	−3.50	5.51D–06	0.1561
<i>Ree10</i>	2206.06560	1.18D–24	1.22D–24	−3.39	5.47D–06	0.1546
<i>Ree12</i>	2211.19617	1.03D–24	1.05D–24	−1.94	5.44D–06	0.1499
<i>Ree13</i>	2213.78692	—	2.85D–24	—	—	—
<i>Ree15</i>	2219.01833	2.21D–24	2.23D–24	−0.90	5.30D–06	0.1388
<i>Ree21</i>	2235.08707	—	7.52D–25	—	—	—
<i>Pff 8</i>	2160.38525	—	1.79D–24	—	—	—
<i>Pff 9</i>	2158.08737	6.18D–25	6.36D–25	−2.91	5.98D–06	—
<i>Pff10</i>	2155.79874	1.95D–24	1.96D–24	−0.51	6.11D–06	—
<i>Pff14</i>	2146.75086	—	1.64D–24	—	—	—
<i>Qef 3</i>	2179.11103	—	9.08D–25	—	—	—
<i>Qef 4</i>	2179.13882	3.49D–24	3.61D–24	−3.44	5.72D–06	—
<i>Qef 6</i>	2179.21514	4.90D–24	4.87D–24	0.61	5.98D–06	0.1696
<i>Qef 7</i>	2179.26351	—	1.75D–24	—	—	—
<i>Qef 8</i>	2179.31925	—	5.47D–24	—	—	—
<i>Qef 9</i>	2179.38164	1.81D–24	1.85D–24	−2.21	5.80D–06	—
<i>Qef10</i>	2179.45104	5.42D–24	5.49D–24	−1.29	5.86D–06	—
<i>Qef11</i>	2179.52752	1.78D–24	1.77D–24	0.56	5.96D–06	0.1489
<i>Qef12</i>	2179.61091	5.01D–24	5.05D–24	−0.80	5.89D–06	0.1452
<i>Qef13</i>	2179.70135	—	1.57D–24	—	—	—
<i>Qef14</i>	2179.79877	4.48D–24	4.31D–24	3.79	6.17D–06	—
<i>Qef15</i>	2179.90330	1.27D–24	1.29D–24	−1.57	5.81D–06	—
<i>Qef16</i>	2180.01500	3.51D–24	3.44D–24	1.99	6.05D–06	0.1346
<i>Qef17</i>	2180.13359	1.04D–24	1.00D–24	3.85	6.16D–06	—
<i>Qef20</i>	2180.53273	—	1.84D–24	—	—	—
<i>Qef22</i>	2180.83519	—	1.23D–24	—	—	—
<i>Qef24</i>	2181.16509	—	7.84D–25	—	—	—
<i>Qef25</i>	2181.34158	—	2.04D–25	—	—	—
<i>Qef26</i>	2181.52519	5.15D–25	4.73D–25	8.16	6.46D–06	—
<i>Qef27</i>	2181.71774	1.22D–25	1.20D–25	1.64	6.02D–06	—
<i>Rff 2</i>	2186.19459	3.11D–24	3.10D–24	0.32	5.70D–06	0.1965
<i>Rff 3</i>	2188.58454	9.86D–25	1.10D–24	−11.56	4.99D–06	0.1911

(continued on next page)

Table 2 (continued)

Line	σ_{obs}	$k_{\sigma}^N_{\text{obs}}$	$k_{\sigma}^N_{\text{calc}}$	O–C%	$ R _{\text{obs}}^2$	$\gamma_{\text{self obs}}^0$
Rff 4	2190.98043	3.45D–24	3.47D–24	−0.58	5.43D–06	0.1735
Rff 6	2195.79712	3.62D–24	3.57D–24	1.38	5.26D–06	0.1651
Rff 7	2198.21814	1.19D–24	1.17D–24	1.68	5.13D–06	0.1682
Rff 8	2200.64772	3.41D–24	3.37D–24	1.17	4.95D–06	0.1591
Rff 10	2205.53626	2.83D–24	2.94D–24	−3.89	4.40D–06	0.1493
Rff 11	2207.99600	8.67D–25	8.86D–25	−2.19	4.28D–06	—
Rff 14	2215.44683	1.65D–24	1.75D–24	−6.06	3.55D–06	0.1475
Rff 17	2223.01882	3.49D–25	3.19D–25	8.60	3.33D–06	—
$v_2 + v_4^1 - v_5^1$						
Pee 2	1839.66051	3.55D–24	3.32D–24	6.48	3.04D–05	0.2213
Pee 3	1837.27846	1.99D–24	1.90D–24	4.52	2.99D–05	0.2022
Pee 4	1834.88150	7.70D–24	7.64D–24	0.78	2.87D–05	0.1827
Pee 5	1832.47013	2.85D–24	3.08D–24	−8.07	2.64D–05	0.1536
Pee 7	1827.60323	3.76D–24	3.78D–24	−0.53	2.83D–05	0.1643
Pee 9	1822.67889	4.06D–24	4.02D–24	0.99	2.88D–05	0.1811
Pee 10	1820.19458	1.20D–23	1.20D–23	0.00	2.86D–05	0.1578
Pee 11	1817.69636	3.86D–24	3.87D–24	−0.26	2.84D–05	0.1577
Pee 12	1815.18338	1.07D–23	1.10D–23	−2.80	2.77D–05	0.1477
Pee 13	1812.65647	3.04D–24	3.44D–24	−13.16	2.52D–05	0.1265
Pee 14	1810.11495	9.20D–24	9.45D–24	−2.72	2.77D–05	0.1408
$v_2 + v_4^1 - v_5^1$						
Ree 2	1851.35101	6.01D–24	5.94D–24	1.16	2.88D–05	0.1933
Ree 3	1853.64461	2.68D–24	2.69D–24	−0.37	2.84D–05	0.1792
Ree 4	1855.92328	9.88D–24	9.90D–24	−0.20	2.84D–05	0.1703
Ree 5	1858.18694	3.80D–24	3.79D–24	0.26	2.85D–05	0.1650
Ree 6	1860.43566	1.25D–23	1.25D–23	0.00	2.85D–05	0.1590
Ree 7	1862.66929	4.45D–24	4.42D–24	0.67	2.87D–05	0.1564
Ree 8	1864.88778	1.42D–23	1.37D–23	3.52	2.97D–05	0.1639
Ree 9	1867.09122	4.59D–24	4.59D–24	0.00	2.85D–05	0.1499
Ree 11	1871.45259	4.35D–24	4.35D–24	0.00	2.85D–05	0.1469
Ree 12	1873.61034	1.24D–23	1.24D–23	0.00	2.86D–05	0.1434
Ree 13	1875.75279	3.79D–24	3.83D–24	−1.06	2.82D–05	0.1393
Ree 14	1877.88003	1.06D–23	1.05D–23	0.94	2.88D–05	0.1391
Ree 15	1879.99174	3.15D–24	3.16D–24	−0.32	2.85D–05	0.1340
Ree 16	1882.08813	8.46D–24	8.39D–24	0.83	2.87D–05	0.1315
Ree 18	1886.23440	6.25D–24	6.30D–24	−0.80	2.82D–05	0.1222
$v_2 + v_4^1 - v_5^1$						
Pff 2	1839.64291	1.02D–24	1.11D–24	−8.82	2.62D–05	0.1883
Pff 3	1837.25376	5.54D–24	5.74D–24	−3.61	2.77D–05	0.1862
Pff 4	1834.85060	2.65D–24	2.57D–24	3.02	2.97D–05	0.1912
Pff 5	1832.43413	9.38D–24	9.35D–24	0.32	2.90D–05	0.1759
Pff 7	1827.56090	1.11D–23	1.15D–23	−3.60	2.80D–05	0.1581
Pff 9	1822.63412	1.23D–23	1.23D–23	0.00	2.90D–05	0.1536
Pff 10	1820.15082	4.31D–24	4.09D–24	5.10	3.08D–05	0.1533
Pff 11	1817.65410	1.21D–23	1.19D–23	1.65	2.98D–05	0.1563
Pff 12	1815.14426	3.87D–24	3.79D–24	2.07	3.00D–05	0.1590

Table 2 (continued)

Line	σ_{obs}	$k_{\sigma}^N_{\text{obs}}$	$k_{\sigma}^N_{\text{calc}}$	o–c%	$ R _{\text{obs}}^2$	$\gamma_{\text{self obs}}^0$
Pff13	1812.62128	1.04D–23	1.06D–23	−1.92	2.89D–05	0.1443
Pff14	1810.08489	3.22D–24	3.25D–24	−0.93	2.93D–05	0.1393
<i>Rff 2</i>	1851.38595	1.89D–24	1.96D–24	−3.70	2.73D–05	0.1781
<i>Rff 3</i>	1853.69334	8.03D–24	8.00D–24	0.37	2.83D–05	0.1839
<i>Rff 4</i>	1855.98694	3.31D–24	3.25D–24	1.81	2.86D–05	0.1778
<i>Rff 5</i>	1858.26666	1.12D–23	1.12D–23	0.00	2.80D–05	0.1673
<i>Rff 6</i>	1860.53248	4.03D–24	4.08D–24	−1.24	2.76D–05	0.1603
<i>Rff 8</i>	1865.02235	4.46D–24	4.44D–24	0.45	2.79D–05	0.1545
<i>Rff 9</i>	1867.24626	1.32D–23	1.34D–23	−1.52	2.73D–05	0.1524
<i>Rff 11</i>	1871.65185	1.26D–23	1.26D–23	0.00	2.75D–05	0.1472
<i>Rff 12</i>	1873.83335	4.11D–24	3.96D–24	3.65	2.85D–05	0.1587
<i>Rff 13</i>	1876.00074	1.09D–23	1.10D–23	−0.92	2.72D–05	0.1439
<i>Rff 14</i>	1878.15390	3.26D–24	3.35D–24	−2.76	2.66D–05	0.1364
<i>Rff 15</i>	1880.29274	8.75D–24	9.01D–24	−2.97	2.65D–05	0.1325
<i>Rff 16</i>	1882.41726	2.74D–24	2.65D–24	3.28	2.81D–05	0.1436
<i>Rff 19</i>	1888.70451	4.31D–24	5.02D–24	−16.47	2.32D–05	0.0916
<i>Rff 21</i>	1892.82342	3.49D–24	3.44D–24	1.43	2.72D–05	0.1191
$(2v_4 + 2v_5)_+^0 \text{II} - v_5^1$						
Pee 6	1904.98093	2.81D–24	3.29D–24	−17.08	6.12D–06	—
Pee 8	1900.47404	3.88D–24	3.74D–24	3.61	7.84D–06	0.1548
Pee10	1896.01826	3.98D–24	3.88D–24	2.51	8.18D–06	0.1519
Pee14	1887.22406	3.45D–24	3.38D–24	2.03	9.25D–06	0.1403
Pee15	1885.04210	1.05D–24	1.05D–24	0.00	9.45D–06	0.1316
Pee16	1882.86408	2.94D–24	2.87D–24	2.38	9.94D–06	0.1343
Pee18	1878.51283	2.32D–24	2.31D–24	0.43	1.05D–05	0.1264
Pee20	1874.15802	1.69D–24	1.75D–24	−3.55	1.08D–05	0.1158
<i>Qef 5</i>	1918.95566	5.32D–24	4.85D–24	8.83	6.85D–06	—
<i>Qef 7</i>	1919.03095	5.45D–24	5.54D–24	−1.65	5.97D–06	—
<i>Qef 9</i>	1919.11811	5.17D–24	5.56D–24	−7.54	5.44D–06	—
<i>Qef11</i>	1919.20882	4.54D–24	5.04D–24	−11.01	5.02D–06	—
<i>Qef12</i>	1919.25256	1.37D–24	1.54D–24	−12.41	4.81D–06	—
<i>Qef13</i>	1919.29273	4.39D–24	4.17D–24	5.01	5.51D–06	—
<i>Qef21</i>	1919.31952	9.74D–25	8.61D–25	11.60	3.82D–06	—
$(2v_4 + 2v_5)_-^0 - v_5^1$						
Pff9	1910.96858	4.24D–24	4.26D–24	−0.47	8.51D–06	0.1527
$(2v_4 + 2v_5)^2 \text{II} - v_5^1$						
Pff17	1892.95282	3.02D–24	3.28D–24	−8.61	2.99D–05	0.1221
Pff21	1883.95462	1.63D–24	1.71D–24	−4.91	3.10D–05	0.1157
Pff23	1879.47637	1.21D–24	1.13D–24	6.61	3.47D–05	—
$4v_5^0 - v_5^1$						
Pee 1	2148.71309	—	1.43D–24	—	—	—

(continued on next page)

Table 2 (continued)

Line	σ_{obs}	$k_{\sigma}^N \text{ obs}$	$k_{\sigma}^N \text{ calc}$	$\text{o-c}\%$	$ R _{\text{obs}}^2$	$\gamma_{\text{self obs}}^0$
Pee 2	2146.37971	—	6.32D–24	—	—	—
Pee 5	2139.48877	3.73D–24	3.75D–24	-0.54	2.37D–05	0.1858
Pee 9	2130.53558	4.35D–24	4.65D–24	-6.90	2.34D–05	0.1504
Pee11	2126.14004	4.55D–24	4.53D–24	0.44	2.60D–05	0.1618
Pee21	2104.45773	1.62D–24	1.57D–24	3.09	3.36D–05	0.1216
Pee22	2102.28038	4.01D–24	3.92D–24	2.24	3.42D–05	0.1232
Pee23	2100.09761	1.08D–24	1.07D–24	0.93	3.44D–05	0.1124
Pee24	2097.90888	2.60D–24	2.62D–24	-0.77	3.49D–05	0.1045
Pee25	2095.71381	7.09D–25	7.01D–25	1.13	3.66D–05	0.1151
Pee28	2089.09248	—	9.28D–25	—	—	—
<i>Qef</i>						
Qef 1	2151.07562	5.92D–24	6.40D–24	-8.11	2.12D–05	0.1880
Qef 2	2151.09436	3.23D–24	3.45D–24	-6.81	2.14D–05	0.1861
Qef 3	2151.12206	1.29D–23	1.38D–23	-6.98	2.11D–05	0.1773
Qef 5	2151.20178	1.76D–23	1.89D–23	-7.39	2.02D–05	0.1630
Qef 8	2151.36853	6.68D–24	6.97D–24	-4.34	1.89D–05	0.1504
Qef11	2151.56090	1.83D–23	1.73D–23	5.46	1.80D–05	0.1540
Qef24	2151.63712	—	5.97D–25	—	—	—
<i>Ree</i>						
Ree 2	2158.23697	4.25D–24	4.20D–24	1.18	2.33D–05	0.1932
Ree 5	2165.56530	3.05D–24	3.11D–24	-1.97	2.30D–05	0.1616
Ree 6	2168.03917	1.03D–23	1.05D–23	-1.94	2.31D–05	0.1593
Ree 7	2170.52633	3.87D–24	3.82D–24	1.29	2.41D–05	0.1562
Ree 9	2175.53532	4.27D–24	4.15D–24	2.81	2.50D–05	0.1502
Ree11	2180.57846	4.38D–24	4.12D–24	5.94	2.66D–05	0.1414
Ree12	2183.10886	1.27D–23	1.20D–23	5.51	2.71D–05	0.1464
Ree16	2193.24267	9.68D–24	8.90D–24	8.06	2.99D–05	0.1329
Ree17	2195.77111	2.90D–24	2.66D–24	8.28	3.07D–05	0.1315
Ree20	2203.32428	5.59D–24	5.26D–24	5.90	3.20D–05	0.1183
Ree21	2205.82828	1.47D–24	1.49D–24	-1.36	3.06D–05	0.1045
Ree22	2208.32469	3.82D–24	3.73D–24	2.36	3.24D–05	0.1096
Ree23	2210.81323	1.01D–24	1.03D–24	-1.98	3.18D–05	0.1047
Ree24	2213.29368	2.45D–24	2.51D–24	-2.45	3.25D–05	0.1192
Ree25	2215.76663	6.65D–25	6.74D–25	-1.35	3.38D–05	0.1182
Ree26	2218.22924	1.57D–24	1.61D–24	-2.55	3.44D–05	0.1001
Ree27	2220.68531	4.02D–25	4.20D–25	-4.48	3.46D–05	0.1045
$4v_5^2 - v_5^1$						
Pee 6	2146.32946	3.66D–24	3.80D–24	-3.83	2.98D–05	0.1743
Pee 9	2139.68063	1.56D–24	1.62D–24	-3.85	2.69D–05	0.1556
Pee10	2137.51066	4.71D–24	4.81D–24	-2.12	2.63D–05	0.1574
Pee11	2135.36597	1.42D–24	1.52D–24	-7.04	2.37D–05	0.1547
Pee13	2131.15930	1.22D–24	1.25D–24	-2.46	2.19D–05	0.1467
Pee14	2129.09999	3.19D–24	3.23D–24	-1.25	2.04D–05	0.1533
Pee15	2127.07214	8.87D–25	8.98D–25	-1.24	1.86D–05	0.1520
Pee18	2121.19211	1.42D–24	1.24D–24	12.68	1.43D–05	0.1400
Pee23	2112.12098	—	1.65D–25	—	—	—

Table 2 (continued)

Line	σ_{obs}	$k_{\sigma}^N \text{ obs}$	$k_{\sigma}^N \text{ calc}$	o–c%	$ R _{\text{obs}}^2$	$\gamma_{\text{self obs}}^0$
$Qfe\ 3$	2160.27763	2.94D–24	2.84D–24	3.40	3.43D–05	0.2140
$Qfe\ 4$	2160.34950	1.09D–23	1.13D–23	−3.67	3.20D–05	0.1798
$Qfe\ 6$	2160.54644	1.48D–23	1.53D–23	−3.38	3.22D–05	0.1692
$Qfe\ 9$	2160.97255	—	5.80D–24	—	—	—
$Qfe11$	2161.34274	5.48D–24	5.56D–24	−1.46	3.27D–05	0.1552
$Qfe13$	2161.77859	4.68D–24	4.93D–24	−5.34	3.15D–05	0.1389
$Qfe14$	2162.02059	1.38D–23	1.36D–23	1.45	3.37D–05	—
$Qfe15$	2162.27829	3.91D–24	4.07D–24	−4.09	3.18D–05	0.1406
$Qfe17$	2162.83916	3.12D–24	3.16D–24	−1.28	3.27D–05	0.1390
$Qfe18$	2163.14167	7.49D–24	8.17D–24	−9.08	3.04D–05	0.1106
$Qfe21$	2164.13252	1.56D–24	1.60D–24	−2.56	3.25D–05	0.1251
$Qfe25$	2165.63063	6.66D–25	6.49D–25	2.55	3.40D–05	0.1172
$Qfe26$	2166.03385	—	1.50D–24	—	—	—
$Ree\ 5$	2174.67493	4.05D–24	3.85D–24	4.94	3.25D–05	0.1915
$Ree\ 8$	2182.20411	1.03D–23	1.08D–23	−4.85	2.66D–05	0.1604
$Ree\ 9$	2184.76203	—	3.37D–24	—	—	—
$Ree10$	2187.34484	8.77D–24	9.20D–24	−4.90	2.43D–05	0.1560
$Ree11$	2189.95568	2.52D–24	2.73D–24	−8.33	2.22D–05	0.1490
$Ree12$	2192.59562	6.71D–24	7.11D–24	−5.96	2.11D–05	0.1494
$Ree13$	2195.26632	1.93D–24	2.00D–24	−3.63	1.99D–05	0.1308
$Ree14$	2197.96816	4.73D–24	4.94D–24	−4.44	1.80D–05	0.1443
$Ree15$	2200.70350	1.28D–24	1.31D–24	−2.34	1.64D–05	0.1350
$Ree17$	2206.27761	7.92D–25	7.40D–25	6.57	1.34D–05	0.1294
$Ree18$	2209.11776	1.81D–24	1.54D–24	14.92	1.20D–05	0.1312
$Ree20$	2214.90738	—	1.11D–24	—	—	—
$Ree21$	2217.85844	—	3.02D–25	—	—	—
$Pff\ 5$	2148.44490	—	3.22D–24	—	—	—
$Pff\ 6$	2146.12499	—	1.39D–24	—	—	—
$Pff11$	2134.65687	5.96D–24	6.22D–24	−4.36	3.33D–05	0.1550
$Pff13$	2130.12554	5.60D–24	5.83D–24	−4.11	3.37D–05	0.1505
$Pff17$	2121.14959	—	4.03D–24	—	—	—
$Pff19$	2116.70179	3.23D–24	3.03D–24	6.19	3.84D–05	0.1404
$Pff22$	2110.07123	—	5.86D–25	—	—	—
$Pff25$	2103.48010	—	8.98D–25	—	—	—
$Qef\ 2$	2160.19570	—	1.70D–24	—	—	—
$Qef\ 4$	2160.25817	4.03D–24	3.88D–24	3.72	3.55D–05	0.1911
$Qef\ 5$	2160.30456	1.40D–23	1.41D–23	−0.71	3.42D–05	0.1748
$Qef\ 6$	2160.36191	5.89D–24	5.39D–24	8.49	3.84D–05	0.1896
$Qef\ 8$	2160.51367	6.19D–24	6.31D–24	−1.94	3.60D–05	0.1551
$Qef12$	2161.00038	7.11D–24	6.47D–24	9.00	4.48D–05	0.1575
$Qef14$	2161.35851	6.44D–24	5.88D–24	8.70	4.75D–05	0.1502
$Qef15$	2161.57148	1.76D–23	1.64D–23	6.82	4.80D–05	0.1449
$Qef16$	2161.80887	5.30D–24	5.03D–24	5.09	4.89D–05	0.1365

(continued on next page)

Table 2 (continued)

Line	σ_{obs}	k_{σ}^N obs	k_{σ}^N calc	o–c%	$ R ^2_{\text{obs}}$	$\gamma_{\text{self obs}}^0$
<i>Qef</i> 20	2163.02239	3.26D–24	3.10D–24	4.91	5.63D–05	0.1330
<i>Qef</i> 21	2163.39486	8.17D–24	7.96D–24	2.57	5.72D–05	0.1260
<i>Qef</i> 23	2164.22392	5.54D–24	5.61D–24	-1.26	5.93D–05	0.1218
<i>Qef</i> 24	2164.67925	1.41D–24	1.54D–24	-9.22	5.72D–05	—
<i>Qef</i> 25	2165.16218	3.62D–24	3.75D–24	-3.59	6.27D–05	0.0938
<i>Qef</i> 26	2165.67057	9.79D–25	1.00D–24	-2.15	6.58D–05	0.1093
<i>Rff</i> 4	2172.10875	3.61D–24	3.84D–24	-6.37	3.04D–05	0.1685
<i>Rff</i> 5	2174.52138	1.13D–23	1.21D–23	-7.08	3.02D–05	0.1633
<i>Rff</i> 6	2176.94173	3.92D–24	4.12D–24	-5.10	3.06D–05	0.1571
<i>Rff</i> 7	2179.37028	1.21D–23	1.24D–23	-2.48	3.11D–05	0.1601
<i>Rff</i> 9	2184.24923	1.18D–23	1.19D–23	-0.85	3.15D–05	0.1588
<i>Rff</i> 10	2186.69935	3.70D–24	3.79D–24	-2.43	3.08D–05	0.1572
<i>Rff</i> 11	2189.15630	1.07D–23	1.07D–23	0.00	3.16D–05	0.1615
<i>Rff</i> 12	2191.61990	3.27D–24	3.29D–24	-0.61	3.11D–05	0.1486
<i>Rff</i> 14	2196.56353	—	2.69D–24	—	—	—
<i>Rff</i> 15	2199.04526	6.90D–24	7.15D–24	-3.62	2.98D–05	0.1376
<i>Rff</i> 16	2201.53102	2.03D–24	2.08D–24	-2.46	2.99D–05	0.1362
<i>Rff</i> 17	2204.02143	5.28D–24	5.36D–24	-1.52	3.00D–05	0.1347
<i>Rff</i> 18	2206.51619	1.50D–24	1.52D–24	-1.33	3.00D–05	0.1317
<i>Rff</i> 19	2209.01440	3.76D–24	3.81D–24	-1.33	2.98D–05	0.1296
<i>Rff</i> 20	2211.51604	1.06D–24	1.05D–24	0.94	3.03D–05	0.1302
<i>Rff</i> 21	2214.02056	2.57D–24	2.57D–24	0.00	3.00D–05	0.1222
<i>Rff</i> 22	2216.52761	—	6.89D–25	—	—	—
<i>Rff</i> 23	2219.03592	—	1.64D–24	—	—	—
<i>Rff</i> 24	2221.54600	—	4.29D–25	—	—	—

^aOnly lines whose position at least could be significantly determined by the multispectrum fitting procedure have been reported; for other lines, the adjustment could not converge, e.g., because of blendings. The lines are given band per band, and by increasing J values inside each branch. In the assignment, the first quoted *e* or *f* character concerns the upper level, and the second concerns the lower level. σ_{obs} is the measured zero pressure line position in cm^{-1} . k_{σ}^N obs is the measured line intensity in cm molecule^{-1} , for pure $^{12}\text{C}_2\text{H}_2$ at 296 K. k_{σ}^N calc is the calculated line intensity in the same units. o–c% is the percentage ratio $100 \times (k_{\sigma}^N \text{ obs} - k_{\sigma}^N \text{ calc})/k_{\sigma}^N \text{ obs}$. $|R|^2_{\text{obs}}$ is the transition dipole moment squared in D^2 ($1\text{D} = 3.33546 \times 10^{-30} \text{ C m}$) deduced from k_{σ}^N obs. $\gamma_{\text{self obs}}^0$ is the measured self-broadening coefficient in $\text{cm}^{-1} \text{ atm}^{-1}$ at 296 K.

this band our multispectrum fitting procedure led to correct line parameters and adjustment of the experimental spectra, so that we do not suspect systematic errors due to the measurement process. This effect could be explained by Coriolis interactions affecting differently the *e* and *f* sub-levels of the $v_5 = 1$ vibrational level, but it is difficult to confirm, considering the set of experimental data available at the present time, as far as intensities of transitions involving the $v_5 = 1$ vibrational level are concerned. Note that, despite very regular rotational dependences, the line intensities of the *Pee* and *Ree* sub-branches of the $(3v_4 + v_5)^2\text{II} - v_4^1$ band (see Fig. 2) cannot be adjusted by Eq. (1), because of strong interactions which also perturb the line positions as stated above.

Self-broadening coefficients γ_{self}^0 have been measured for 371 lines. In Ref. [3], we saw that there does not exist any significant vibrational dependence. In Fig. 12, we have gathered all the self-broadening coefficients obtained in this work and in Ref. [3]. Adjusting these values by a

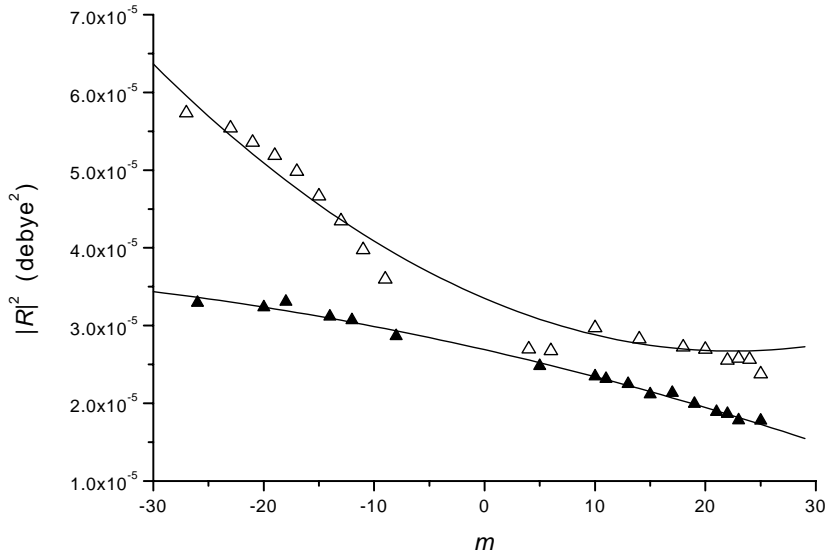


Fig. 2. Variation of the transition dipole moment squared $|R|^2$ (in D^2 , $1D = 3.33546 \times 10^{-30} \text{ C m}$), vs. m , for the $(3v_4 + v_5)^2\text{II} - v_4^1$ band of $^{12}\text{C}_2\text{H}_2$. Open triangles are for Pee and Ree lines, and black triangles for Pff and Rff lines. The curves have been calculated using the constants found in this work (see Table 3).

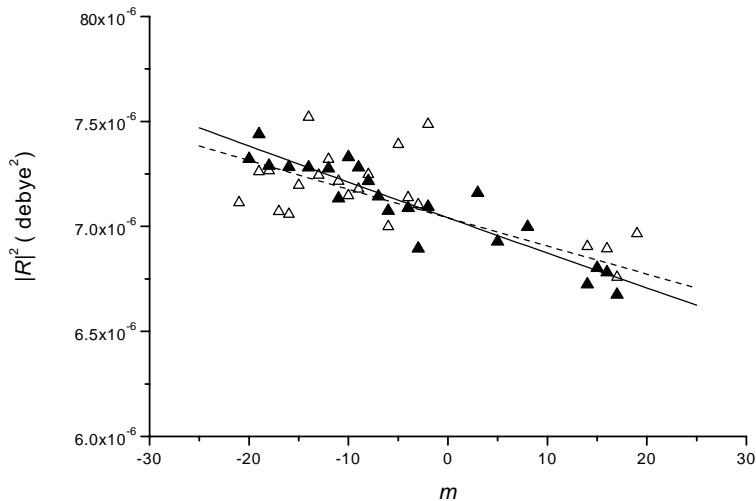


Fig. 3. Variation of the transition dipole moment squared $|R|^2$ (in D^2 , $1D = 3.33546 \times 10^{-30} \text{ C m}$), vs. m , for the $v_2 + v_5^1 - v_4^1$ band of $^{12}\text{C}_2\text{H}_2$. Open triangles are for Pee and Ree lines, and black triangles for Pff and Rff lines. The curves have been calculated using the constants found in this work (see Table 3): the dashed straight line is for the ee sub-band, and the continuous straight line for the ff sub-band.

polynomial expansion vs. $|m|$, we found

$$\begin{aligned} \gamma_{\text{self}}^0(T) = & [0.2031(19) - 0.00642(45)|m| + 0.000181(29)m^2 \\ & - 2.93(58) \times 10^{-6}|m|^3] \times (T_0/T)^{0.75} \end{aligned} \quad (3)$$

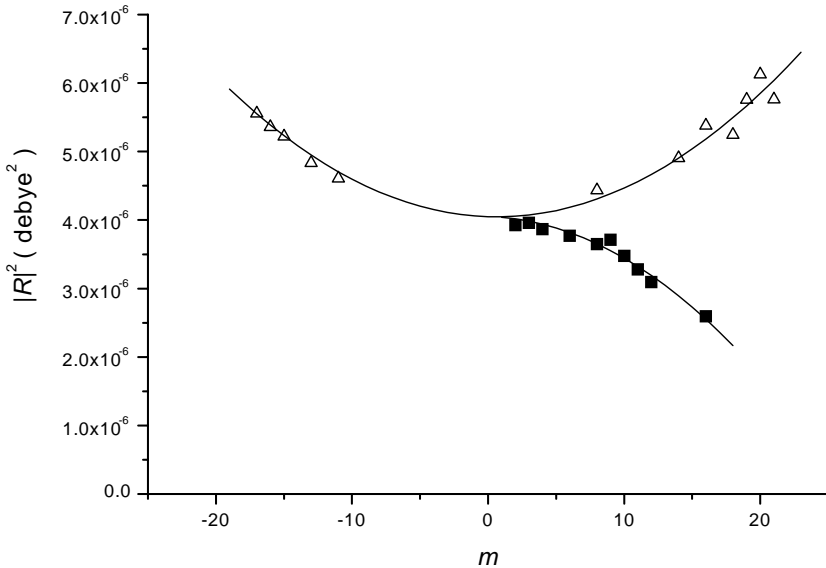


Fig. 4. Variation of the transition dipole moment squared $|R|^2$ (in D^2 , $1\text{D} = 3.33546 \times 10^{-30} \text{ C m}$), vs. m , for the $(v_4 + 3v_5)^0_+ - v_4^1$ band of $^{12}\text{C}_2\text{H}_2$. Open triangles are for Pee and Ree lines, and black squares for Qef lines. The curves have been calculated using the constants found in this work (see Table 3).

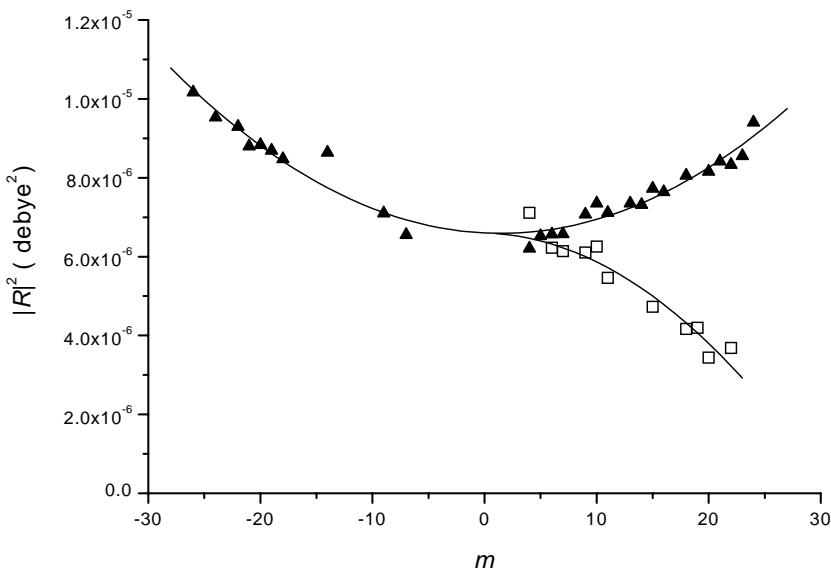


Fig. 5. Variation of the transition dipole moment squared $|R|^2$ (in D^2 , $1\text{D} = 3.33546 \times 10^{-30} \text{ C m}$), vs. m , for the $(v_4 + 3v_5)^0_- - v_4^1$ band of $^{12}\text{C}_2\text{H}_2$. Black triangles are for Pff and Rff lines, and open squares for Qfe lines. The curves have been calculated using the constants found in this work (see Table 3).

with, between parenthesis, 1 SD in unit of the last digit, T_0 being equal to 296 K. The exponent 0.75 comes from Varanasi et al. [11]. Note that Eq. (5) of Ref. [3], obtained from a set of data smaller than in the present work, leads to very similar results. Thus, we propose

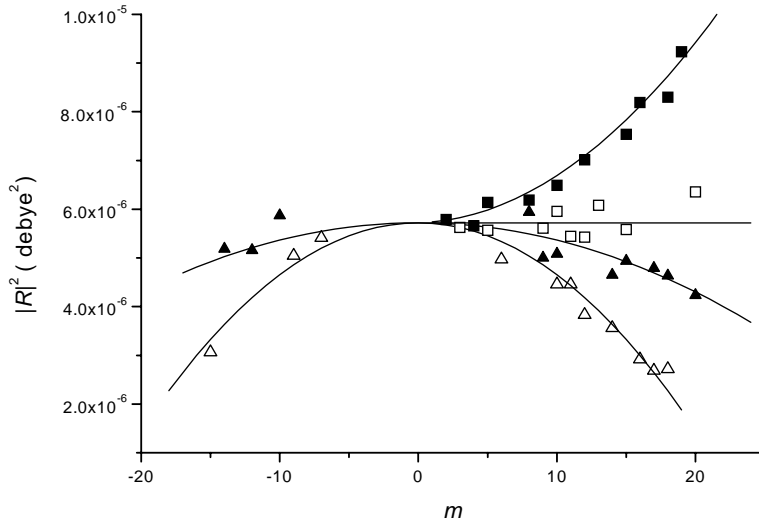


Fig. 6. Variation of the transition dipole moment squared $|R|^2$ (in D^2 , $1D = 3.33546 \times 10^{-30} \text{ C m}$), vs. m , for the $(v_4 + 3v_5)^2 \text{II} - v_4^1$ band of $^{12}\text{C}_2\text{H}_2$. Open triangles are for Pee and Ree lines, black triangles for Pff and Rff lines, open squares for Qfe lines, and black squares for Qef lines. The curves have been calculated using the constants found in this work (see Table 3).

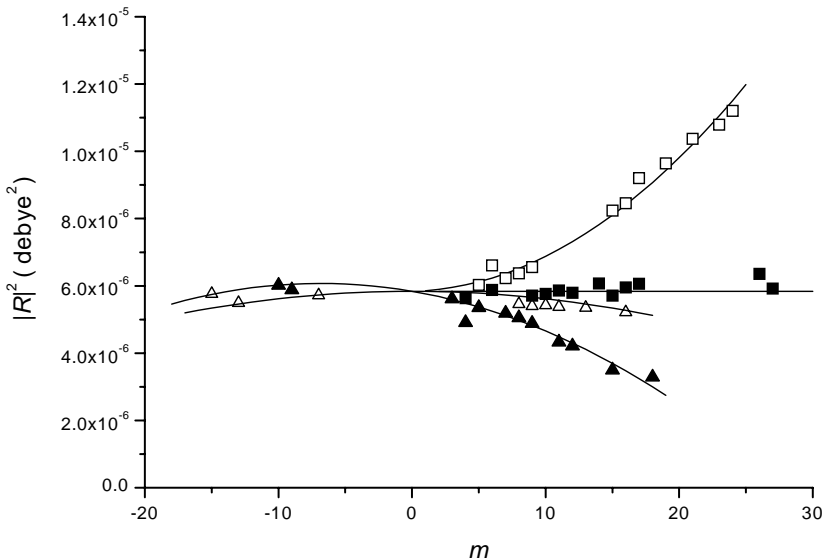


Fig. 7. Variation of the transition dipole moment squared $|R|^2$ (in D^2 , $1D = 3.33546 \times 10^{-30} \text{ C m}$), vs. m , for the $(v_4 + 3v_5)^2 \text{I} - v_4^1$ band of $^{12}\text{C}_2\text{H}_2$. Open triangles are for Pee and Ree lines, black triangles for Pff and Rff lines, open squares for Qfe lines, and black squares for Qef lines. The curves have been calculated using the constants found in this work (see Table 3).

Eq. (3) for calculating the self-broadening coefficient of all lines in all bands of acetylene, up to $|m|$ equal to 33, and with $\gamma_{\text{self}}^0 = 0.0812 \text{ cm}^{-1} \text{ atm}^{-1}$ for $|m|$ greater than or equal to 34. The rotational dependence of γ_{self}^0 given by this formula can be considered as

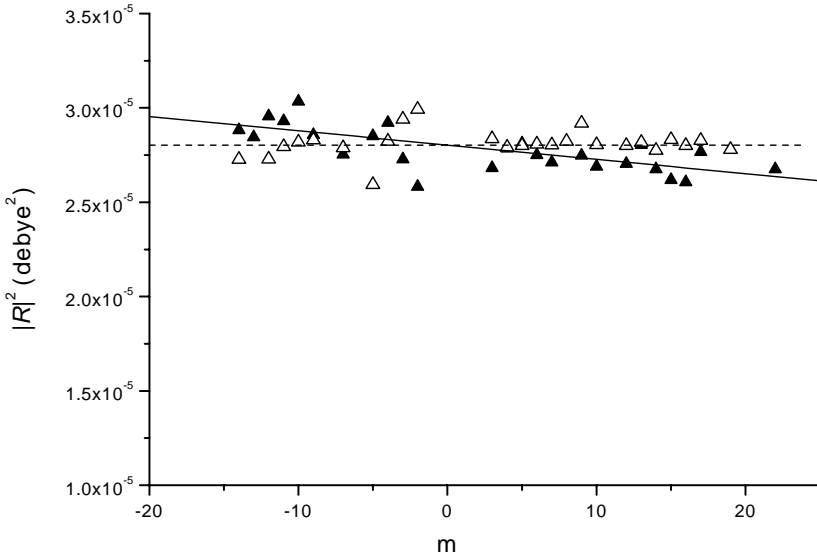


Fig. 8. Variation of the transition dipole moment squared $|R|^2$ (in D^2 , $1D = 3.33546 \times 10^{-30} \text{ C m}$), vs. m , for the $v_2 + v_4 - v_1^1$ band of $^{12}\text{C}_2\text{H}_2$. Open triangles are for *Pee* and *Ree* lines, and black triangles for *Pff* and *Rff* lines. The curves have been calculated using the constants found in this work (see Table 3): the dashed straight line is for the *ee* sub-band, and the continuous straight line for the *ff* sub-band.

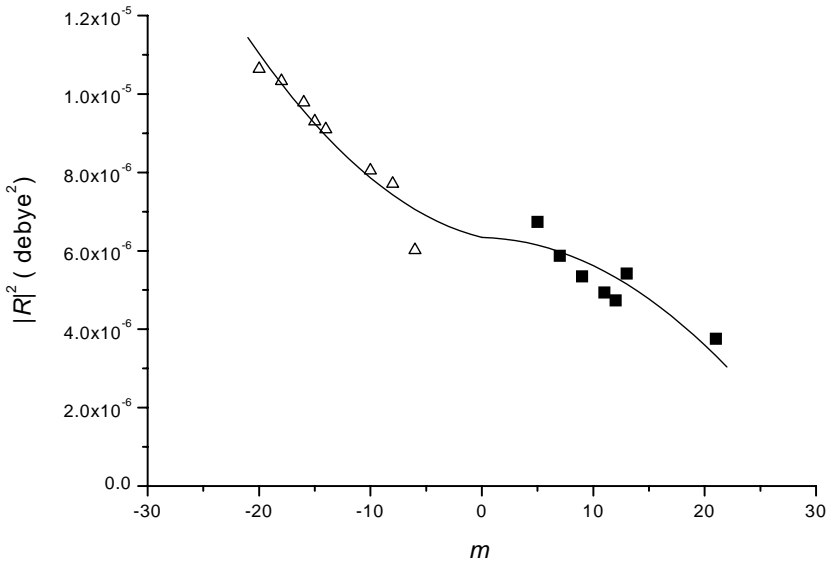


Fig. 9. Variation of the transition dipole moment squared $|R|^2$ (in D^2 , $1D = 3.33546 \times 10^{-30} \text{ C m}$), vs. m , for the $(2v_4 + 2v_5)^0_+ \text{II} - v_5^1$ band of $^{12}\text{C}_2\text{H}_2$. Open triangles are for *Pee* lines, and black squares for *Qef* lines. The curves have been calculated using the constants found in this work (see Table 3).

accurate within an uncertainty of $\pm 3\%$, with the assumption that it is applied to bands for which there is no vibrational dependence, not too high J lines, and inside a temperature range close to room temperature.

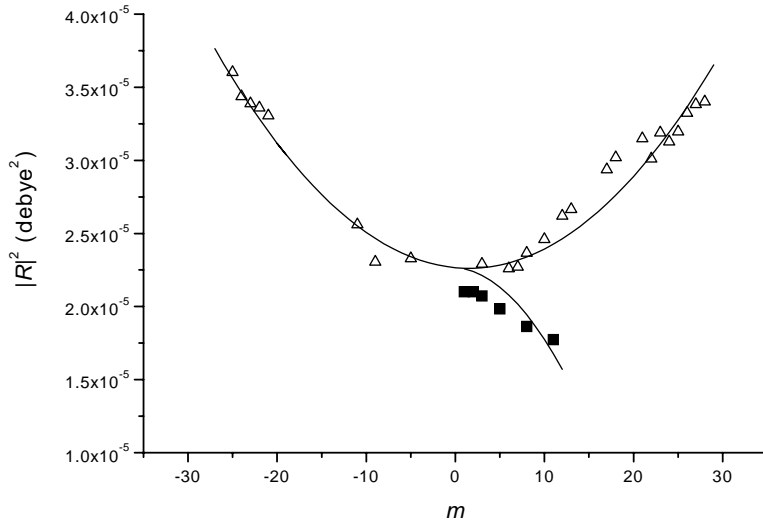


Fig. 10. Variation of the transition dipole moment squared $|R|^2$ (in D^2 , $1D = 3.33546 \times 10^{-30} \text{ C m}$), vs. m , for the $4v_5^0 - v_5^1$ band of $^{12}\text{C}_2\text{H}_2$. Open triangles are for *Pee* and *Ree* lines, and black squares for *Qef* lines. The curves have been calculated using the constants found in this work (see Table 3).

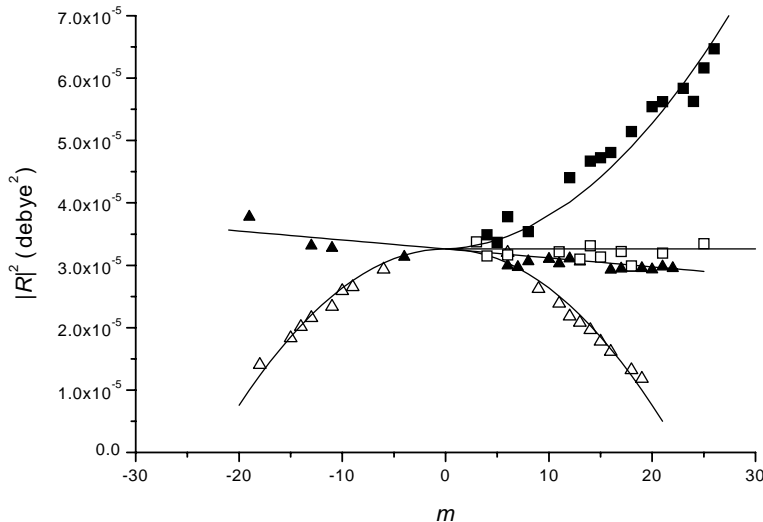


Fig. 11. Variation of the transition dipole moment squared $|R|^2$ (in D^2 , $1D = 3.33546 \times 10^{-30} \text{ C m}$), vs. m , for the $4v_5^2 - v_5^1$ band of $^{12}\text{C}_2\text{H}_2$. Open triangles are for *Pee* and *Ree* lines, black triangles for *Pff* and *Rff* lines, open squares for *Qfe* lines, and black squares for *Qef* lines. The curves have been calculated using the constants found in this work (see Table 3).

Self-shifting coefficients δ_{self}^0 are tentatively given for 122 lines (see Table 4). They have been plotted in Figs. 13–15 for some interesting bands. The confidence intervals (1 SD) of the retained δ_{self}^0 values are around $\pm 0.002 \text{ cm}^{-1} \text{ atm}^{-1}$, but they can attain about $\pm 0.006 \text{ cm}^{-1} \text{ atm}^{-1}$ for some

Table 3

Summary of $^{12}\text{C}_2\text{H}_2$ vibrational transition dipole moments squared, Herman-Wallis coefficients, and band intensities, obtained for 3 cold bands [3] and 15 hot bands in the 5- μm spectral region (this work)^a

Band	Center	$ R_0 ^2$	A_1^{RP}	A_2^{RP}	A_2^Q	S_V		
$3v_5^1$	2169.166	10.828(67)	-3.54(19)	-0.29(10)	-0.66(20)	810		
$(2v_4 + v_5)^1\text{II}$	1940.003	7.685(69)	-15.11(35)	-0.53(19)	1.26(58)	514		
$(2v_4 + v_5)^1\text{I}$	1959.697	2.060(34)	-2.60(70)	2.66(59)	-6.07(90)	142		
$(3v_4 + v_5)_+^0 - v_4^1$	1948.906	18 ₃ (—) ^b	—	—	—	61.9		
$(3v_4 + v_5)_-^0 - v_4^1$	1972.151	3.99(47)	0	-57(14)	13(11)	13.9		
$(3v_4 + v_5)^2\text{II} - v_4^1$	<i>ee</i>	1945.126	34.0(34)	-18.0(34)	4.0(28)	—	58.5	
	<i>ff</i>	1945.126	27.36(47)	-11.96(57)	-0.91(47)	—	46.9	
$(3v_4 + v_5)^2\text{I} - v_4^1$	<i>ee</i>	1973.283	4.7 ₈ (12 ₀)	0	-43(13)	—	16.7	
	<i>ff</i>			0	17(26)	—		
$v_2 + v_5^1 - v_4^1$	<i>ee</i>	2090.213	7.157(51)	-1.92(73)	0	—	26.4	
	<i>ff</i>			-2.41(81)	0	—		
$(v_4 + 3v_5)_+^0 - v_4^1$	2146.104	4.12(12)	-1.6(14)	11.9(16)	-13.6(24)	15.6		
$(v_4 + 3v_5)_-^0 - v_4^1$	2171.957	6.71(17)	-2.11(99)	7.33(92)	-10.1(11)	25.7		
$(v_4 + 3v_5)^2\text{II} - v_4^1$	<i>ee</i>	2156.792	5.81(14)	0	-18.6(19)	<i>fe</i>	0	22.1
	<i>ff</i>			0	-6.2(17)	<i>ef</i>	15.4(20)	
$(v_4 + 3v_5)^2\text{I} - v_4^1$	<i>ee</i>	2179.100	5.934(96)	0	-3.8(19)	<i>fe</i>	16.19(94)	22.8
	<i>ff</i>			-11.7(33)	-8.5(26)	<i>ef</i>	0	
$v_2 + v_4^1 - v_5^1$	<i>ee</i>	1844.372	28.49(23)	0	0	—	52.4	
	<i>ff</i>			-2.7(10)	0	—		
$(2v_4 + 2v_5)_+^0\text{II} - v_5^1$	1918.863	6.44(82)	-11(37)	13(19)	-10.3(60)	12.3		
$(2v_4 + 2v_5)_-^0 - v_5^1$	1932.033	8.5 ₄ (—) ^b	—	—	—	16.47		
$(2v_4 + 2v_5)^2\text{II} - v_5^1$	<i>ff</i> ^c	1932.289	32. ₅ (2 ₅) ^c	—	—	—	62.6 ^c	
$4v_5^0 - v_5^1$		2151.065	23.03(74)	-2.5(12)	8.14(98)	-19.7(77)	49.4	
$4v_5^2 - v_5^1$	<i>ee</i>	2160.208	33.15(68)	0	-19.2(15)	<i>fe</i>	0	71.3
	<i>ff</i>			-4.4(19)	0	<i>ef</i>	14.7(11)	

^aThe quoted band centers, in cm^{-1} , are from Plíva [4]. The vibrational transition dipole moments squared $|R_0|^2$ are in 10^{-6}D^2 ($1\text{D} = 3.33546 \times 10^{-30} \text{C m}$). The Herman-Wallis coefficients are defined by Eqs. (1) and (2). The A_1^{RP} coefficients have to be multiplied by 10^{-3} , and the A_2^{RP} and A_2^Q coefficients have to be multiplied by 10^{-4} ; when a zero value is reported, the corresponding coefficient was fixed to zero in the fit. Between parentheses, the quoted 95% statistical confidence intervals are 2 SD in units of the last digit. The band intensities S_V are in $10^{-23} \text{cm}^{-1}/(\text{molecule cm}^{-2})$ at 296 K and in natural abundances. In case of ℓ -type doubling, and if the two sub-bands were fitted simultaneously, $|R_0|^2$ is reported once, and the quoted S_V value is the whole intensity of the band (not to be confused with the intensities reported for each sub-band, when the two sub-bands could be fitted separately).

^bValue of $|R_0|^2$ obtained from only one line.

^cValue of $|R_0|^2$ obtained from only three *Pff* lines. S_V is the total band intensity.

lines. Note that the measurement of pressure-shifts is particularly difficult when the lines are weak because of the noise level (as is the case for many lines in the present work), and taking into account the fact that the maximum pressure of our spectra is only 50 Torr (our spectra were not especially recorded with the aim of deducing pressure-shifting coefficients). A discussion is necessary about the effect of the uncertainty of the pressure-shifting coefficient determination, on the deduced zero-pressure line position. In the “general” version [8] of the multispectrum fitting procedure (MSF), in which all the line parameters (including the zero-pressure line position and the

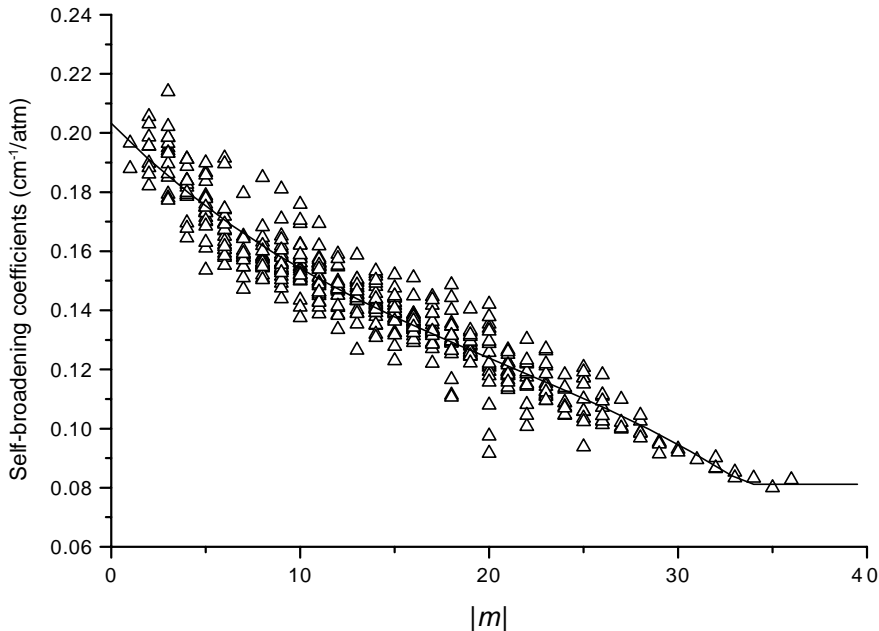


Fig. 12. Self-broadening coefficients γ_{self}^0 of $^{12}\text{C}_2\text{H}_2$ vs. $|m|$, in $\text{cm}^{-1} \text{ atm}^{-1}$ at 296 K. Plotted are all our results concerning the 3 cold bands studied in Ref. [3] and the 15 hot bands studied in the present work: one sees that these values are well gathered around an adjusted polynomial expansion (continuous line); cf. Eq. (3).

self-shifting coefficient) are common to all spectra, the information allowing the determination of the zero-pressure line position comes from the low-pressure spectra, whereas the information leading to the pressure-shifting coefficient comes from the high-pressure spectra. In our case, an accurate adjustment of the zero-pressure line position is forced by the numerous low-pressure spectra taken into account, since even a noticeable error in the pressure-shifting coefficient, for which the information comes mainly from the 50-Torr spectrum, has a totally negligible consequence in the final zero-pressure line position. The previous conclusion would no longer be valid if our set of spectra contained much more high-pressure spectra than low-pressure spectra (by “high” pressure, we mean a pressure high enough to induce non-negligible pressure-shifts, but too low to lead to a very accurate determination of these pressure-shifts). However, even in this case, this drawback can be avoided by using a “reduced” version [8] of the MSF procedure, in which the line positions are not constrained in each spectrum (consequently, pressure-shifting coefficients cannot be deduced), other line parameters remaining common to all spectra. Then, zero-pressure line positions can be obtained considering only the line positions adjusted for the low-pressure spectra. Let us discuss a typical example. The tests we performed on a weak line (poor SNR), for which a significant and relatively large self-shifting coefficient of $0.012 \text{ cm}^{-1} \text{ atm}^{-1}$ was found (confidence interval: $0.014 \text{ cm}^{-1} \text{ atm}^{-1}$), led to conclusions that we checked with other similar lines:

- First, the “general” MSF procedure applied to all spectra (i.e., including the 50-Torr spectrum) gave a zero-pressure line position identical to that obtained by the same method, but disregarding

Table 4

Self-shifting coefficients measured at room temperature, for hot bands of $^{12}\text{C}_2\text{H}_2$ in the 5- μm spectral region^a

Line	σ_{obs}	$\delta_{\text{self obs}}^0$	SD	Line	σ_{obs}	$\delta_{\text{self obs}}^0$	SD
$(3v_4 + v_5)_+^0 - v_4^1$ <i>Qef20</i>	1951.49101	-5.49	3.38				
$(3v_4 + v_5)_-^0 - v_4^1$ <i>Qfe 9</i>	1972.70409	-2.55	2.21	<i>Qfe11</i>	1972.88785	-1.08	2.57
$(3v_4 + v_5)^2\text{II} - v_4^1$ <i>Pee11</i>	1919.93952	-2.24	0.90	<i>Pff 8</i>	1926.35236	-2.23	2.92
<i>Pee13</i>	1915.44460	-2.19	0.93	<i>Pff12</i>	1917.09168	1.05	0.89
<i>Pee15</i>	1910.93702	-0.54	0.55	<i>Pff14</i>	1912.48543	-1.08	0.81
<i>Pee19</i>	1901.85420	-1.35	0.74	<i>Pff18</i>	1903.31092	1.93	0.81
<i>Pee21</i>	1897.27439	0.74	0.97				
<i>Pee23</i>	1892.66951	-1.35	1.59				
<i>Ree 3</i>	1954.65251	-4.70	4.17	<i>Rff 9</i>	1968.96809	-6.25	5.16
<i>Ree 5</i>	1959.50405	-6.73	2.56	<i>Rff14</i>	1981.03696	-8.62	2.59
<i>Ree 9</i>	1969.28797	-5.25	3.82	<i>Rff16</i>	1985.87757	-6.30	3.20
<i>Ree13</i>	1979.06574	-8.60	2.17	<i>Rff18</i>	1990.72098	-8.38	2.19
<i>Ree17</i>	1988.74504	-7.93	2.21	<i>Rff20</i>	1995.56303	-6.57	2.30
<i>Ree19</i>	1993.53792	-6.56	2.82				
<i>Ree21</i>	1998.29918	-6.34	2.10				
<i>Ree23</i>	2003.02909	-4.92	2.37				
$(3v_4 + v_5)^2\text{I} - v_4^1$ <i>Rff10</i>	1999.61650	-1.65	2.02				
$v_2 + v_5^1 - v_4^1$ <i>Pee11</i>	2063.80453	-2.60	0.91	<i>Pff 4</i>	2080.70395	-1.60	1.48
<i>Pee12</i>	2061.34402	-2.37	1.94	<i>Pff 6</i>	2075.88097	0.84	2.14
<i>Pee15</i>	2053.90375	0.20	0.84	<i>Pff 7</i>	2073.45290	-2.25	2.19
<i>Pee17</i>	2048.89545	-3.66	3.04	<i>Pff 8</i>	2071.01380	-2.83	0.78
<i>Pee19</i>	2043.84896	-4.19	6.40	<i>Pff 9</i>	2068.56370	0.68	1.79
<i>Pee21</i>	2038.76448	-0.96	1.73	<i>Pff12</i>	2061.14798	-0.94	0.71
				<i>Pff14</i>	2056.15000	0.97	1.12
				<i>Pff16</i>	2051.10914	0.91	0.84
				<i>Pff20</i>	2040.90001	-0.17	1.36
<i>Ree13</i>	2122.03232	0.02	1.26	<i>Rff 4</i>	2101.85096	-4.13	1.85
<i>Ree15</i>	2126.40764	-1.00	0.87	<i>Rff13</i>	2122.06591	-0.42	3.15
				<i>Rff15</i>	2126.42868	-0.77	2.56
				<i>Rff16</i>	2128.59227	-2.32	1.56
$(v_4 + 3v_5)_+^0 - v_4^1$ <i>Peel11</i>	2121.26792	0.68	0.90	<i>Ree15</i>	2185.90288	-0.13	1.70
<i>Peel13</i>	2116.94732	1.63	1.17				
<i>Peel15</i>	2112.65948	0.89	1.12				
<i>Peel17</i>	2108.39073	-0.96	1.29				

Table 4 (continued)

Line	σ_{obs}	$\delta_{\text{self obs}}^0$	SD	Line	σ_{obs}	$\delta_{\text{self obs}}^0$	SD
$(v_4 + 3v_5)_-^0 - v_4^1$							
Pff18	2130.41564	-1.45	1.32	Rff10	2198.37662	-2.90	1.08
				Rff12	2203.24185	-4.71	0.86
Rff 4	2183.87312	-1.22	2.15	Rff14	2208.11250	-3.53	1.27
Rff 6	2188.68727	-2.90	5.34	Rff20	2222.69356	-1.71	2.15
Rff 9	2195.94818	-3.95	4.13	Rff22	2227.52454	-1.94	2.82
$(v_4 + 3v_5)^2 \text{II} - v_4^1$							
Ree 9	2181.36715	-4.19	1.61	Rff 8	2178.37623	-7.73	2.49
Ree11	2186.56900	-5.80	4.50	Rff14	2193.11961	-3.79	1.70
				Rff16	2198.08092	-0.41	3.59
Pff14	2124.46331	-3.12	3.58				
$(v_4 + 3v_5)^2 \text{I} - v_4^1$							
Qfe19	2182.74079	-1.64	1.16	Ree 7	2198.49740	-1.67	1.11
				Ree15	2219.01833	0.91	2.09
$v_2 + v_4^1 - v_5^1$							
Ree 4	1855.92328	5.27	0.93	Rff 3	1853.69334	3.55	1.19
Ree 6	1860.43566	4.01	0.62	Rff 5	1858.26666	4.88	0.87
Ree 7	1862.66929	0.72	1.27	Rff 9	1867.24626	2.64	0.55
Ree 8	1864.88778	-3.68	1.32	Rff11	1871.65185	-0.45	0.60
Ree 9	1867.09122	4.67	1.26	Rff13	1876.00074	-0.78	0.63
Ree11	1871.45259	-1.29	1.00	Rff14	1878.15390	0.39	1.62
Ree12	1873.61034	-1.27	0.42	Rff15	1880.29274	-2.79	0.78
Ree13	1875.75279	0.85	1.16	Rff16	1882.41726	-0.82	4.20
Ree14	1877.88003	-4.14	0.41				
Ree15	1879.99174	0.10	1.29				
Ree16	1882.08813	-3.54	0.51				
Ree18	1886.23440	-6.68	0.83				
$(2v_4 + 2v_5)_+^0 \text{II} - v_5^1$							
Pee10	1896.01826	0.84	1.70	Pee14	1887.22406	-1.47	1.17
$(2v_4 + 2v_5)_-^0 - v_5^1$							
Pff 9	1910.96858	-3.08	1.75				
$4v_5^0 - v_5^1$							
Pee24	2097.90888	-1.55	1.43	Ree16	2193.24267	-4.00	0.52
				Ree20	2203.32428	-3.19	0.70
Ree 6	2168.03917	-1.93	1.05	Ree22	2208.32469	-2.49	2.86
Ree12	2183.10886	-3.91	0.61	Ree26	2218.22924	-3.04	1.92

(continued on next page)

Table 4 (continued)

Line	σ_{obs}	$\delta_{\text{self obs}}^0$	SD	Line	σ_{obs}	$\delta_{\text{self obs}}^0$	SD
$4v_5^2 - v_5^1$							
Pee10	2137.51066	-1.76	1.24	Pff13	2130.12554	1.94	1.71
Pee13	2131.15930	-1.40	3.97	Pff19	2116.70179	0.04	0.79
Pee14	2129.09999	6.19	2.11	Qfe23	2164.22392	-0.42	1.46
Qfe21	2164.13252	-2.90	3.93	Rff9	2184.24923	-0.29	0.54
Ree 8	2182.20411	-3.44	0.73	Rff10	2186.69935	-2.45	1.09
Ree10	2187.34484	-1.99	1.53	Rff11	2189.15630	-3.43	1.54
Ree11	2189.95568	1.05	2.02	Rff15	2199.04526	-5.34	0.95
Ree12	2192.59562	-2.26	1.47	Rff16	2201.53102	-3.78	1.76
Ree14	2197.96816	-4.43	0.82	Rff17	2204.02143	-5.76	0.78
Ree18	2209.11776	2.58	2.34	Rff19	2209.01440	-2.50	1.02
				Rff21	2214.02056	-3.96	1.66

^aThe lines are given band per band, and by increasing J values inside each branch. In the assignment, the first quoted e or f character concerns the upper level, and the second concerns the lower level. σ_{obs} is the measured zero-pressure line position in cm^{-1} . $\delta_{\text{self obs}}^0$ is the measured self-shifting coefficient in $10^{-3} \text{ cm}^{-1} \text{ atm}^{-1}$ at about 296 K. SD, is the 68% confidence interval, i.e., 1 SD, of $\delta_{\text{self obs}}^0$, in $10^{-3} \text{ cm}^{-1} \text{ atm}^{-1}$.

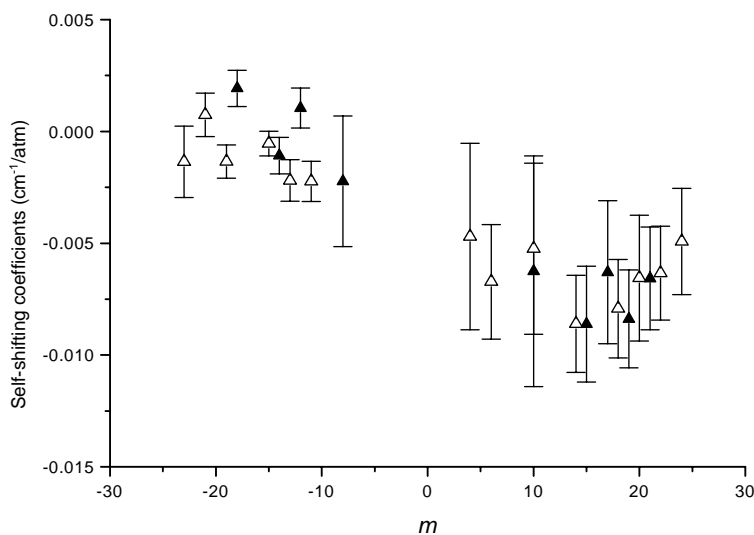


Fig. 13. Self-shifting coefficients δ_{self}^0 of $^{12}\text{C}_2\text{H}_2$ vs. m in $\text{cm}^{-1} \text{ atm}^{-1}$ at about 296 K, for the $(3v_4 + v_5)^2\text{II} - v_4^1$ band. Open triangles are for Pee and Ree lines, and black triangles for Pff and Rff lines. The error bars are a ± 1 SD statistical uncertainty.

the 50-Torr spectrum (discrepancy smaller than 10^{-6} cm^{-1}), showing that taking into account the 50-Torr spectrum does not worsen the zero-pressure line position, even in the case where the retrieved self-shifting coefficient has an anomalously large value.

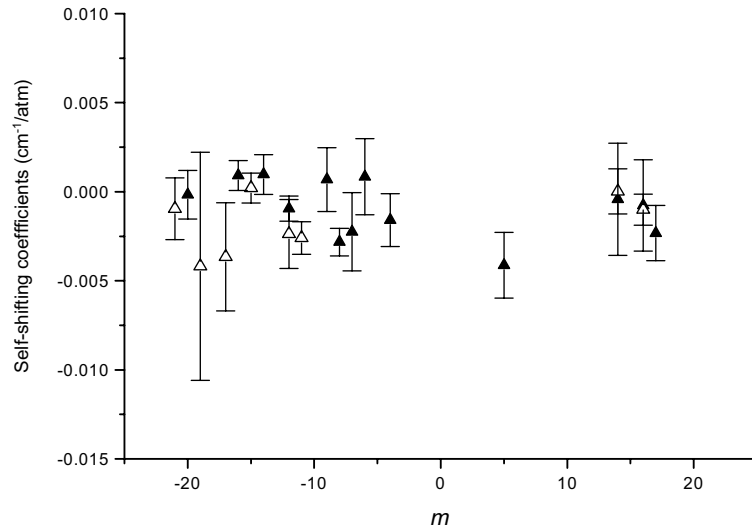


Fig. 14. Self-shifting coefficients δ_{self}^0 of $^{12}\text{C}_2\text{H}_2$ vs. m in $\text{cm}^{-1} \text{atm}^{-1}$ at about 296 K, for the $\nu_2 + \nu_5^1 - \nu_4^1$ band. Open triangles are for Pee and Ree lines, and black triangles for Pff and Rff lines. The error bars are a ± 1 SD statistical uncertainty.

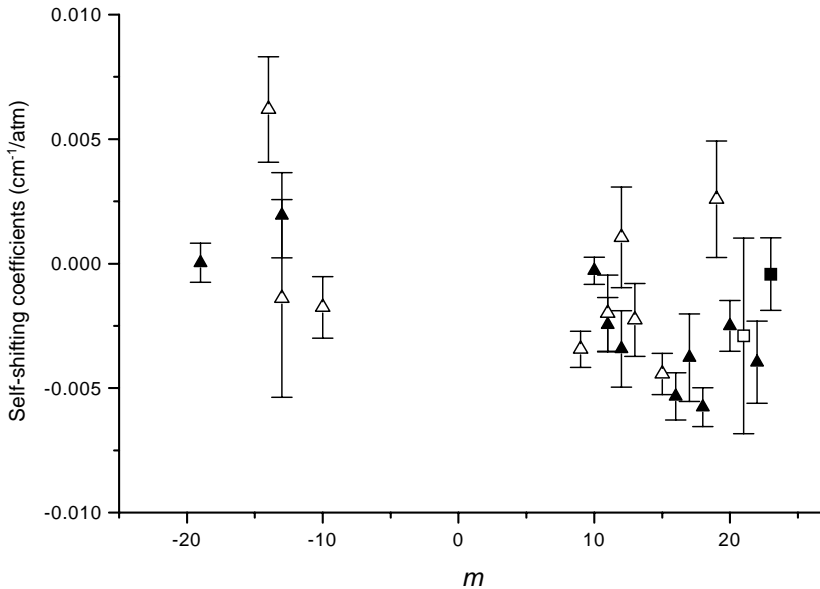


Fig. 15. Self-shifting coefficients δ_{self}^0 of $^{12}\text{C}_2\text{H}_2$ vs. m in $\text{cm}^{-1} \text{atm}^{-1}$ at about 296 K, for the $4\nu_5^2 - \nu_3^1$ band. Open triangles are for Pee and Ree lines, black triangles for Pff and Rff lines, the black square for a Qef line, and the open square for a Qfe line. The error bars are a ± 1 SD statistical uncertainty.

- Second, the “reduced” MSF procedure (with or without the 50-Torr spectrum) gave line positions in low-pressure spectra very close together (discrepancies smaller than $5 \times 10^{-5} \text{ cm}^{-1}$), showing that the relative calibration of the wavenumber scales of the involved spectra is correct.

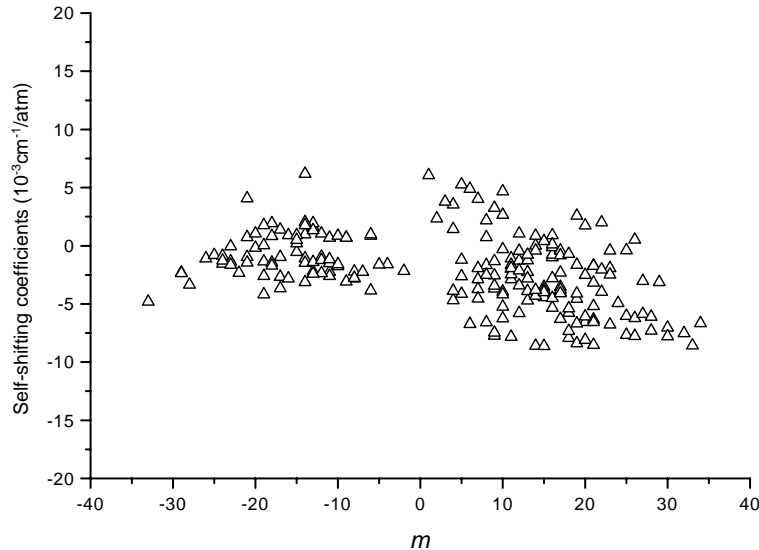


Fig. 16. Self-shifting coefficients δ_{self}^0 of $^{12}\text{C}_2\text{H}_2$ vs. m in $\text{cm}^{-1}\text{atm}^{-1}$ at about 296 K, for all the 5- μm region bands studied in Ref. [3] and in the present work.

- Third, these line positions obtained by the “reduced” MSF procedure do not differ from the zero-pressure line positions obtained from the “general” MSF procedure by more than 10^4 cm^{-1} , a discrepancy well inside our stated $2 \times 10^{-4} \text{ cm}^{-1}$ mean accuracy.
- Fourth, the self-shifting coefficient determined from the “reduced” MSF line positions in the low-pressure spectra and in the 50-Torr spectrum is very close to the value deduced by the “general” MSF procedure (0.011 vs. $0.012 \text{ cm}^{-1}\text{atm}^{-1}$). This shows the coherence of the method: the information allowing the determination of δ_{self}^0 comes from the 50-Torr spectrum and leads to very similar results whatever the method is, but, as this information is very poor, those results can be erroneous, showing that the uncertainty in the absolute values of δ_{self}^0 is certainly larger than the confidence intervals.

For all these reasons, few significant values were finally retained (see Table 4). Fig. 16 contains all the results obtained in the present work, together with the results obtained in Ref. [3]. Taking into account the uncertainties, neither vibrational dependence nor rotational dependence could be observed. As estimations of self-shifting coefficients can be useful for wavenumber calibration purposes, it is interesting to give the average value calculated from our results: $-0.0022 \text{ cm}^{-1}\text{atm}^{-1}$ at about 296 K.

4. Synthetic spectrum

The bands occurring in the studied spectral region involve energy levels coupled by anharmonic resonances, and vibrational or rotational essential ℓ -type resonances, so that they are interesting for further theoretical calculations, using effective operator models enabling the calculation of the whole

spectrum of acetylene [6,7]. The concerned anharmonic interactions are due to the 44/55 and ${}^{\prime}44/55$ accidental vibrational resonances (see, e.g., Refs. [5,6]), i.e., the so-called bending–bending second order Darling-Dennison type interactions, which occur between levels with $\Delta v_1 = \Delta v_2 = \Delta v_3 = 0$, $\Delta v_4 = \pm 2$, $\Delta v_5 = \mp 2$. Thus we thought it useful to gather all the data concerning this region, and available at the present time, in a HITRAN-format line list. This file¹ is of course evolving and will be updated as soon as new computations become available. Between 1810 and 2255 cm⁻¹, the ${}^{12}\text{C}_2\text{H}_2$ bands taken into account to set up this file are the 3 cold bands studied in Ref. [3] and the 15 hot bands studied in the present paper. At the present time, no resonance was taken into account in the calculation of the line positions and line intensities.

The line positions have been calculated as explained in Section 3, and no extrapolation was performed for the final list: the last line in each branch corresponds to the larger J value observed either by Plíva or by us. In the case where the maximum J value observed by Plíva is greater than ours, Plíva's calculated line positions (possibly slightly shifted) have sometimes been chosen rather than ours for the lines we could not analyze. For the bands for which no adjustment was possible, Plíva's calculated line positions were chosen. Note that because of strong interactions mentioned in Ref. [4], only the Pff and Rff sub-branches of the $(2v_4 + 2v_5)^2\text{II} - v_5^1$ band are observable and consequently were calculated. Conversely, it is worth noticing that we observed many P lines in the $v_2 + v_5^1 - v_4^1$ and $v_2 + v_4^1 - v_5^1$ bands, whereas none of them is present in Ref. [4]. The lower-state energy values, E'' , were taken from HITRAN [12].

The line intensities have been calculated, in cm molecule⁻¹ at 296 K, and in natural abundances as is usual for HITRAN (97.760% for ${}^{12}\text{C}_2\text{H}_2$), using the constants listed in Table 3. For J greater than the J value corresponding to our last measured intensity, namely J_{\max} , the line intensities were calculated extrapolating Eqs. (1) and (2), but for some bands, they were calculated fixing the transition dipole moment squared at its value calculated for J_{\max} . The self-broadening coefficients have been calculated using Eq. (3). Among the experimental results available for air-broadening effects (see bibliography in Table 1 of Ref. [3]), we have chosen the results of Lambot et al. [13] and Bouanich et al. [14] concerning v_5^1 lines. The temperature-dependence exponent, $n = 0.75$, of the air-broadening coefficient is a mean value obtained from Refs. [14–16] which showed that n is noticeably J -dependent, since its experimental values vary from about 0.85 to 0.60 according to J between 1 and 30. Despite this variation, the same rough mean value 0.75 was incorporated for all the lines involved in the 5-μm region. The air-broadening coefficients are smoothed values obtained from Refs. [13,14] for $|m|$ between 1 and 34; they are given in Table 5, at $T_0 = 296$ K. For $|m|$ greater or equal to 34, γ_{air}^0 is fixed to 0.0450 cm⁻¹ atm⁻¹ at 296 K. The value of γ_{air}^0 for $m=0$ was extrapolated. Note that recent measurements from Sun and Varanasi [17] should allow the improvement of these data. As far as air-shifting coefficients are concerned, we are only aware of the N₂-shifting coefficients measured by Babay et al. [18] for v_5^1 lines at room temperature (between 290 and 295 K). Although these values are noticeably J -dependent, we chose a rough mean value -0.001 cm⁻¹ atm⁻¹ for all lines.

The accuracy codes follow the HITRAN convention and are: 3 for calculated line positions (error range between 0.001 and 0.01 cm⁻¹), 6 for calculated line intensities and broadening coefficients (between 2% and 5%). Note that the intensity accuracy code has been degraded (code 4, i.e.,

¹ Available upon request to the authors. This file can be down-loaded from the web-site <http://CFA-www.Harvard.edu/HITRAN/updates.html>.

Table 5

Air-broadening coefficients γ_{air}^0 of $^{12}\text{C}_2\text{H}_2$ lines, obtained from the smoothed values published by Lambot et al. [13] and Bouanich et al. [14]. The unit is $10^{-3} \text{ cm}^{-1} \text{ atm}^{-1}$ at 296 K

$ m $	γ_{air}^0	$ m $	γ_{air}^0
0	117.7	18	71.9
1	111.4	19	70.4
2	104.3	20	68.8
3	98.5	21	67.1
4	94.0	22	65.3
5	90.3	23	63.5
6	87.5	24	61.6
7	85.2	25	59.7
8	83.4	26	57.8
9	82.0	27	56.0
10	80.8	28	54.1
11	79.6	29	52.4
12	78.7	30	50.7
13	77.7	31	49.1
14	76.8	32	47.7
15	75.6	33	46.3
16	74.6	34	45.0
17	73.3		

between 10% and 20%, or code 5, i.e., between 5% and 10%) for a strongly perturbed sub-band (*Pee*, *Ree*, and *Qfe* sub-branches of the $(3v_4 + v_5)^2\text{II} - v_4^1$ band), and for some bands ($(3v_4 + v_5)_+^0 - v_4^1$, $(3v_4 + v_5)_-^0 - v_4^1$, $(3v_4 + v_5)^2\text{I} - v_4^1$, $(2v_4 + 2v_5)_-^0 - v_5^1$, and $(2v_4 + 2v_5)^2\text{II} - v_5^1$), whose intensity is known only from a few individual line intensities.

To conclude this paper, let us recall that a large number of line parameters have been obtained in this work for 18 bands of acetylene in the 5-μm region, using a multispectrum fitting procedure. Particularly, together with improved absolute line positions, absolute intensities have been measured for 540 lines (mean accuracy $\pm 5\%$). These data will be useful for further theoretical calculations. Numerous self-broadening and self-shifting coefficients have also been measured, and an approximate value of the self-collisional narrowing coefficient, namely $\beta^0 = 0.064 \pm 0.015$ (1SD) $\text{cm}^{-1} \text{ atm}^{-1}$ at about 296 K [3], has been determined, improving noticeably the knowledge of pressure effects on C_2H_2 lines belonging to various bands.

Acknowledgements

The authors acknowledge Pr. A. Barbe, Dr. M.-R. De Backer-Barily, Mrs. X. Thomas and P. Von der Heyden for their contribution to this work.

References

- [1] Plateaux JJ, Barbe A, Delahaigue A. Reims high resolution Fourier transform spectrometer. Data reduction for ozone. *Spectrochim Acta* 1995;51A:1153–69.

- [2] Régalias L. Mesures à l'aide d'un spectromètre par transformation de Fourier, des intensités et coefficients d'élargissement de molécules d'intérêt atmosphérique. Étude des précisions: application à N₂O, H₂O, O₃. Thèse, Université de Reims-Champagne-Ardenne, Reims, France, 1996.
- [3] Jacquemart D, Mandin JY, Dana V, Régalias-Jarlot L, Thomas X, Von der Heyden P. Multispectrum fitting measurements of line parameters for 5 μm cold bands of acetylene. *JQSRT* 2002;75:397–422.
- [4] Plíva J. Spectrum of acetylene in the 5-micron region. *J Mol Spectrosc* 1972;44:145–64.
- [5] Plíva J. Molecular constants for the bending modes of acetylene ¹²C₂H₂. *J Mol Spectrosc* 1972;44:165–82.
- [6] Perevalov VI, Lobodenko EI, Teffo JL. Reduced effective hamiltonian for global fitting of C₂H₂ rovibrational lines. In Proceedings of the XIIth Symposium and School on High-Resolution Molecular Spectroscopy. Saint Petersburg, Russia, 1–5 July 1996. SPIE 1997; 3090: 143–9.
- [7] Teffo JL, Lyulin OM, Perevalov VI, Lobodenko EI. Application of the effective operator approach to the calculation of ¹²C¹⁶O₂ line intensities. *J Mol Spectrosc* 1998;187:28–41.
- [8] Jacquemart D, Mandin JY, Dana V, Picqué N, Guelachvili G. A multispectrum fitting procedure to deduce molecular line parameters. Application to the 3-0 band of ¹²C¹⁶O. *Eur Phys J D* 2001;14:55–69.
- [9] Jacquemart D, Claveau C, Mandin JY, Dana V. Line intensities of hot bands in the 13.6 μm spectral region of acetylene ¹²C₂H₂. *JQSRT* 2001;69:81–101.
- [10] Gamache RR, Kennedy S, Hawkins RL, Rothman LS. Total internal partition sums for molecules in the terrestrial atmosphere. *J Mol Struct* 2000;517–518:407–25.
- [11] Varanasi P, Giver LP, Valero FPJ. Infrared absorption by acetylene in the 12–14 μm region at low temperatures. *JQSRT* 1983;30:497–504.
- [12] Rothman LS, Rinsland CP, Goldman A, Massie ST, Edwards DP, Flaud JM, Perrin A, Camy-Peyret C, Dana V, Mandin JY, Schroder J, McCann A, Gamache RR, Wattson RB, Yoshino K, Chance KV, Jucks KW, Brown LR, Nemtchinov V, Varanasi P. The HITRAN molecular spectroscopic database and HAWKS (Hitran Atmospheric Workstation): 1996 edition *JQSRT* 1998;60:665–710.
- [13] Lambot D, Blanquet G, Bouanich JP. Diode laser measurements of collisional broadening in the v₅ band of C₂H₂ perturbed by O₂ and N₂. *J Mol Spectrosc* 1989;136:86–92.
- [14] Bouanich JP, Lambot D, Blanquet G, Walrand J. N₂- and O₂-broadening coefficients of C₂H₂ IR lines. *J Mol Spectrosc* 1990;140:195–213.
- [15] Bouanich JP, Blanquet G, Populaire JC, Walrand J. Nitrogen broadening of acetylene lines in the v₅ band at low temperature. *J Mol Spectrosc* 1998;190:7–14.
- [16] Bouanich JP, Blanquet G, Walrand J. Oxygen broadening of acetylene lines in the v₅ band at low temperature. *J Mol Spectrosc* 1999;194:269–77.
- [17] Sun C, Varanasi P. *JQSRT*, in press.
- [18] Babay A, Ibrahim M, Lemaire V, Lemoine B, Rohart F, Bouanich JP. Line frequency shifting in the v₅ band of C₂H₂. *JQSRT* 1998;59:195–202.